（表紙）

表　　題　心筋細胞成熟における細胞外マトリックスの機能解明

論 文 の 区 分　博士課程

著　者　名　Nawin　Chanthra

担当指導教員氏名　花園　豊　教授

所　　属　自治医科大学大学院医学研究科
専攻　人間生物学系
専攻分野　生体分子医学
専攻科　再生医科学

２０２０年１月１０日申請の学位論文

ELUCIDATION OF THE EFFECTS OF EXTRACELLULAR MATRICES ON CARDIOMYOCYTE MATURATION

心筋細胞成熟における細胞外マトリックスの機能解明

Nawin Chanthra, MSc

A Thesis Submitted in Partial Fulfillment of the Requirements for the Degree of Doctor of Philosophy

Division of Regenerative Medicine, Center for Molecular Medicine
Jichi Medical University

Academic Year 2019

Abstract

Introduction

Pluripotent stem cell-derived cardiomyocytes (PSC-CMs) are promising cells for research and medical applications. Although PSC-CMs are efficiently obtained with a directed cardiac differentiation method, they solely display fetal-like phenotypes and arrest at embryonic state of maturation. A lack of applicable high-throughput method providing distinguished parameters for determining the maturity of cardiomyocytes (CMs) hampers the progress of understanding molecular mechanisms of CM maturation and producing adult-like mature CMs from PSC-CMs. Several studies have shown that extracellular matrices (ECMs) might play pivotal roles in CM maturation. However, it is largely unknown how ECMs regulate the maturation and which ECM is superior to others. Therefore, I aimed to develop assessment tools for CM maturation and to assess the effects of ECMs on CM maturation in this study.

Results

As a ton of study have shown that fluorescence reporter lines built a significant impact on the field of stem cell research, especially providing better insights in biology and function of PSC-CMs both *in vitro* and *in vivo*. Thus, I hoped that a fluorescence maturation reporter would use for the determination of CM maturation as well. Previously, our group has identified Myom2 as a candidate, because its expression gradually increases from late-embryonic to postnatal heart. Here, I first knocked a red fluorescence protein (RFP) reporter gene into 3' end of *Myom2* in mouse embryonic stem cells, namely Myom2-RFP. Then, I examined the expression profiles of Myom2-RFP during cardiac differentiation. I found that RFP was not detected in PSC-CMs right after differentiation at day 10, while a prolonged culture of PSC-CMs, which enhanced maturation, significantly increased both RFP^+ cells and RFP intensity from day 21 to 28 of cardiac differentiation. Furthermore, I intensively compared structure, function, and transcription between RFP^+ and RFP^- cells to validate the reporter. I found that RFP^+ cells showed a longer length of sarcomere, increased cell size and aspect ratio, become more binuclear, as well as improved calcium handling property. Along with transcriptome analysis, cardiac genes and specific genes in biological processes of adult CMs were highly upregulated in RFP^+ cells. These results suggested that the reporter line can be used as a reporter for CM maturation.

I identified that ECMs including laminin, collagen, and fibronectin, showed temporal upregulation during maturation of the hearts. To test if the ECMs had any impacts on CM maturation, I examined the dose-dependencies of the ECMs on Myom2-RFP. To this end, I plated Myom2-RFP PSC-CMs at day 10 of differentiation on different concentrations of ECMs ranging from 0.125 μg/cm^2 - 1 μg/cm^2, and cultured up to day 38 of cell culture. I found that high concentrations of the ECMs, especially laminin-511/521, significantly increased Myom2-RFP expression. In addition, morphological, physiological, and functional analysis demonstrated that laminin-511/521 promoted PSC-CMs towards adult-like mature CMs such as long sarcomere length, increase cell size, increase percent of binuclear cell, inducing connexin 43 to lateral cell-axis, improving mitochondrial function, as well as improving calcium handling and cell shortening properties.

Next, I performed an RNA sequencing to assess the maturation statuses of PSC-CMs plated on laminin-511/521. The transcriptomes of the PSC-CMs were compared to mouse heart counterparts. The result demonstrated that PSC-CMs plated on laminin-511 at day 38 had the highest maturation score compared to gelatin and laminin-521. Nevertheless, specific genes related to CMs were slightly upregulated in laminin-511/521 such as cardiac marker (*Tnnt2*), sarcomere proteins (*Actc1, Mybpc2*, *Mybpc3*, *Myh7*, *Myl2*), transcriptional regulator (*Ankrd23*), and calcium handling (*Casq2*).

Conclusion

Laminin-511/521 promoted morphological, physiological, functional, and transcriptional changes of PSC-CMs, and also enhanced Myom2-RFP expression. Therefore, this study highlight laminin-511/521 as potent enhancers for CM maturation.

Keywords:
Pluripotent stem cell-derived cardiomyocytes (PSC-CMs), Cardiomyocytes (CMs), Extracellular matrices (ECMs)

This thesis is dedicated to all members of my family, teachers, and lovely friends, whose supported me from the beginning to the end of my doctoral degree.

Table of Contents

List of Figures

List of Tables

Chapter 1
Aim overview

Recent advances enable efficient differentiation of cardiomyocytes (CMs) from pluripotent stem cells (PSCs) for broad applications. However, pluripotent stem cell-derived CMs (PSC-CMs) only display immature phenotypes. Although several studies have shown that extracellular matrices (ECMs) might play pivotal roles in CM maturation, the maturity of PSC-CMs with those ECMs compared to *in vivo* heart remain unknown as no assessment tool is available. Therefore, my ultimate goal is to generate fully mature CMs for the breakthrough applications of advanced medicine. To this end, I first attempted to develop novel assessment tools for CM maturation and determine the effects of ECMs on CM maturation. To achieve the goal, the aims of this study are divided into two parts.

AIM 1: Development of assessment tools for CM maturation.

A lack of assessment tools for CM maturation is a key road brick to obtain fully mature CMs. Thus, I have developed qualitative and quantitative methods to assess CM maturation as explained below.

1.1) Generation of a qualitative method for CM maturation

As a lack of assessment tools for CM maturation is a major obstacle to obtain mature PSC-CMs effectively, I first generated a fluorescent CM maturation reporter line. Our transcriptome data indicated that *Myom2*, encoding to M-protein, one of sarcomere protein, starts to express around late-embryonic stage and increases subsequently. Therefore, I decided to knock-in the red fluorescence protein (RFP) to 3' end of *Myom2* genomic locus, hereafter called Myom2-RFP. To achieve knock-in efficiency, I used CRISPR/Cas9 system, a genome-editing tool, to generate double-strand break at the target region. Myom2 is localized to the M-line of the sarcomere. Thus, I expected that RFP would be observed in the same region as Myom2 protein which located *in vivo*.

1.2) Development of a quantitative method for CM maturation

Previously, our group has developed a microarray-based quantitative assay for CM maturation[1]. However, this method is expensive. Thus, I recently updated the method with Quant-seq, using poly T primer to synthesize cDNA and sequence predominantly 3' end of mRNA. This approach requires less read depth and allows more multiplexing samples per run with affordable cost. With the update method, I have set a weight for each gene to calculate the maturation score. The maturation score is sum of the expression level of each gene (transcript per million reads, TPM) multiplied by the weight. With this method, I could determine the exact maturation status of PSC-CMs, and also examine specific gene expressions related to CMs.

AIM 2: Evaluation of the effects of ECMs on CM maturation

Mouse PSC-CMs exhibited more mature properties on native cardiac ECMs such as laminin, collagen, and fibronectin, which are secreted from cardiac fibroblasts. Here, I examined if ECMs promote CM maturation using qualitative and quantitative methods. And if so, what degree of maturation PSC-CMs achieved by the ECMs. To this end, PSC-CMs generated from the reporter line were plated on different types of ECMs at day 10 of cardiac differentiation. Then, morphological, physiological, and functional analysis, were conducted at day 38, to evaluate the effects of those ECMs on CM maturation. Moreover, I also corrected RNA from all of the conditions and performed RNA-sequencing to assess the maturation degree of PSC-CMs plated on ECMs. With these methods, I could identify potent ECMs which are able to enhance maturation of the PSC-CMs *in vitro*.

Chapter 2
Introduction

Stem cell research has a long history since the 1960s. Date back to that time period, James E. Till, a biophysicist, and Ernest A. McCulloch, a hematologist, accidentally found that irradiated mice which conducted intravenous injection of bone marrow, formed the colonies of proliferating cells in their spleen. Those cells are blood-forming progenitor cells that have the ability to repopulate blood cells, resulting in engagement towards using bone marrow transplantation for hematopoietic diseases[2]. Since the discovery, the regarding researches have been reported for isolation, identification, and characterization of different types of stem cells. To date, the major advances and discoveries in stem cell research have been generated by using PSCs.

2.1) Pluripotent stem cells

PSCs are the cells that have two important properties including self-renewal and potency (Fig. **1**). The self-renewal is an ability of PSCs that can produce daughter cells indefinitely, and those cells still have similar properties of progenitor cells (Fig. **1a**). In specific conditions or under particular signals, PSCs are able to undergo any cell types which are derived from all three germ layers (ectoderm, mesoderm, and endoderm) of body, which is defined as "differentiation"[3] (Fig. **1b**).

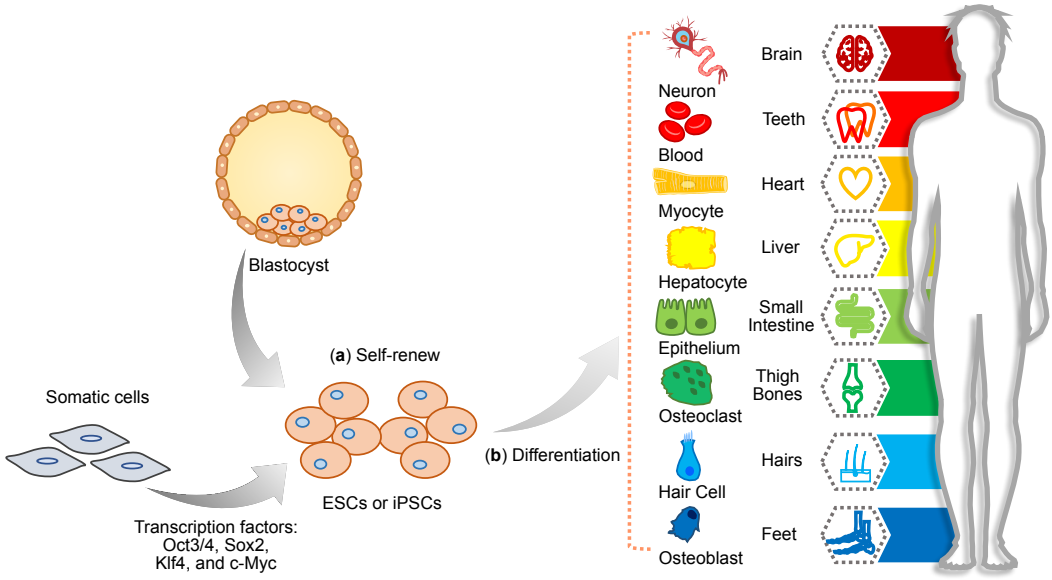

Figure 1. Properties of PSCs.
PSCs are cells that have possess a nearly unlimited (**a**) self-renewal ability and (**b**) potentially differentiate into numerous cell types of an organism.

PSCs can be classified into two types including embryonic stem cells (ESCs) and induced pluripotent stem cells (iPSCs). ESCs are derived from the inner cell mass of embryo at the blastocyst stage[4,5] (Fig. **1**). In addition to ESCs, PSCs can be obtained by inducing different transcriptional factors (such as Oct3/4, Sox2, Klf4, and c-Myc) into adult somatic cells, or well known as "iPSCs"[6,7]. Both ESCs and iPSCs are able to maintain a pluripotent state and expand in a dish.

2.2) Characteristics of PSC-CMs

PSC-CMs have indisputable cardiomyogenic potential and therefore have been intensively investigated as a potential cardiac regenerative therapy[8]. With cardiac differentiation, CMs can be efficiently derived from PSCs in high yield[9]. Although PSC-CMs hold a great promising for a wide range of medical applications, it is well known that PSC-CMs display morphological, physiological, and functional characteristics like fetal CMs rather than adult CMs under culturing-system currently. Different properties between immature and adult CMs are showed in Fig. **2** and summarized in Table **1**.

2.2.1) Morphology

During heart development, cardiac muscle cells undergo sophisticated series of structural changes and eventually lead to adult phenotypes (Fig **2a** and Table **1**). Adult CMs exhibit a large number of length to width ratio (aspect ratio), binucleation, and form complex ultrastructure such as T-tubules and sarcoplasmic reticulum along Z-line of the sarcomere[10]. Adult CMs not only exhibit Z, I, H, A, and M bands, but also have long sarcomere length (2.2 μm) and highly organized[10]. Moreover, N-cadherin, $Na_v1.5$, and connexin 43 (Cx43) are localized to the intercalated disk of CMs[11] (Fig **2c**). In contrast, PSC-CMs tend to be round, mononucleated, and have shorter sarcomere length (1.6 μm) and disorganized[10]. These cells also do not show T-tubules formation, while simply exhibit Z and I-bands[10].

2.2.2) Contractile apparatus

Sarcomere is a crucial unit for cardiac contraction. Thus, measuring sarcomere gene expressions such as cardiac troponin T (cTnT), α-actinin, myosin heavy chain (MHC: human, β isoform; mouse, α isoform), are highly expressed to the maturation of PSC-CMs[12–14]. The mentioned genes are not only expressed in adult CMs, but also relatively upregulated in immature CMs. Electron microscope has illustrated that PSC-CMs have immature structural characteristics with various degrees of sarcomere

organization[15,16]. In addition, adult CMs are more quiescent in terms of beating, but stimulated adult CMs provide greater force of contraction, upstroke and conduction velocities[10,17]. Indeed, PSC-CMs generate lower conduction and upstroke velocities but remain beat spontaneously[10,17] (Table **1**).

2.2.3) Metabolism

Corresponding with the increasing of mitochondria in adult CMs, the oxidative capacity is increased, which represents to switch in metabolic substrates from glucose to fatty acid[18]. In early heart development, around 80% of energy is produced by glycolysis. When CMs become mature, fatty acid β-oxidation increases and becomes a major source for energy production. In contrast, PSC-CMs rely on glycolysis rather than fatty acid β-oxidation[19] (Table **1**).

2.2.4) Calcium handling property

Calcium handling property is one of the most common parameters that is characterized in PSC-CMs (Fig. **2b**). Several studies have been reported that PSC-CMs express important calcium handling proteins which impact calcium transients[13,14,20–22]. For instance, previous work showed that transduction of PSC-CMs with a regulatory protein for calcium handling, calsequestrin (encoded from *Casq2* gene), increased peak amplitude, upstroke velocity and time to decay, suggesting that calsequestrin is implicated to functional maturation of the PSC-CMs[23]. In addition to regulatory protein for calcium handling, the function of sarcoplasmic reticulum for calcium storage is also critical for calcium handling property. Previous studies found that PSC-CMs have dissimilar functional sarcoplasmic reticulum compared to adult CMs in several animal models such as mice[24,25], rat[26,27], and rabbit[28]. Moreover, characterizations of PSC-CMs have demonstrated that calsequestrin expression has also supported the presence of functional SR-dependent calcium handling[13,14]. Altogether, it is plausible that distingue calcium handling properties may be caused by a variety in maturation status of tested PSC-CMs.

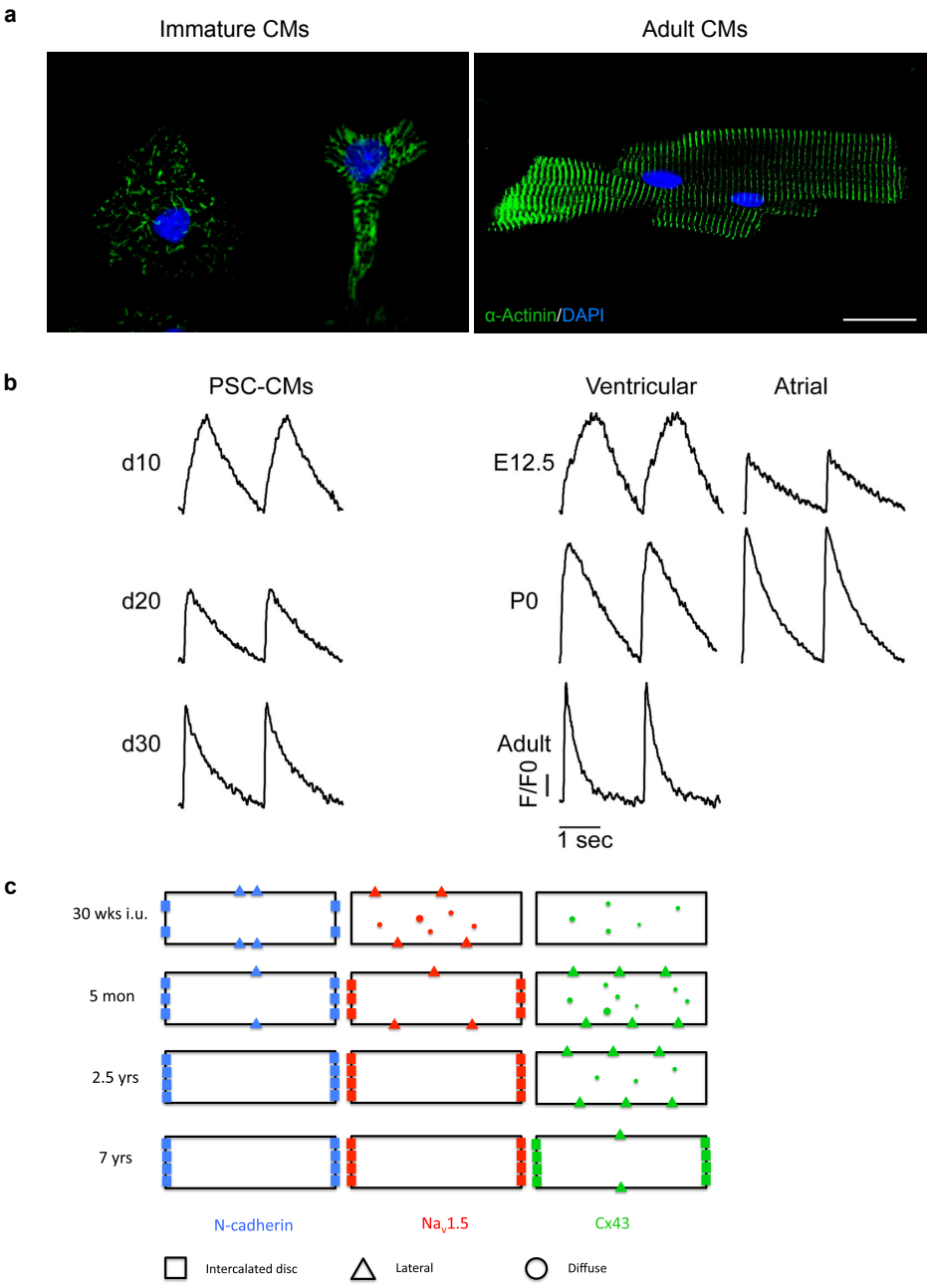

Figure 2. Different characteristics between immature and mature CMs.

(**a**) Immature CMs are round or polygonal in shape and have disorganized sarcomere pattern, whereas adult CMs are longer and show more organized sarcomere. Scale bar = 20 μm. (**b**) Representative Ca^{2+} transients of embryonic day 12.5 (E12.5), neonatal, adult CMs, and PSC-CMs. PSC-CMs show dissimilarity of Ca^{2+} transient peaks compared to those of adult CMs. Fig. **1b** was modified from Uosaki *et al*[1]. (**c**) Schematic summary of protein localizations during heart development ranging from 30 weeks in utero (wks i.u.) to 7 years postnatal; N-cadherin (blue), $Na_v1.5$ (red), and connexin 43 (Cx43, green). Fig. **2c** was modified from Vreeker *et al*[11].

Table 1. Summary of different properties between immature and mature CMs.

Properties	Parameters	Fetal CMs	PSC-CMs	Adult CMs	Ref.
Morphology	Shape	Round or polygonal	Round or polygonal	Rod and elongated	*16,29,30*
	Nucleation	Mononucleated	Mononucleated	Binucleated: Human ~25% Mouse ~ 91.5%	*31,32*
Sarcomere	Appearance	Disorganized	Disorganized	Organized	*30*
	Length	Shorter (~1.6 μm)	Shorter (~1.6-1.8 μm)	Longer (~2.2 μm)	*30,33*
Mitochondria	Structure	Round and small	Slender and small	Oval in shape	*15,34,35*
	Distribution	Close to nucleus and circumference	Close to nucleus and circumference	Along the direction of sarcomere	*15*
Metabolic substrate	Substrate	Glucose	Glucose	Fatty acid	*18,19*
Myofibrillar isoform switch	Titin	N2BA	N2BA	N2B	*30,36*
	Troponin I	TNNI1	TNNI1	cTnI	*30,36*
	MHC: Human Mouse	β > α	β ≈ α	β >> α α >> β	*30,36* *37*
T-tubules	Present	Absent	Absent	Present	*33*
Gap junction	Distribution	Circumference	Circumference	Intercalated disc	*11*
Conduction velocity	Velocity	~30 cm/s	10-20 cm/s	60 cm/s	*38,39*
Electrophysiology properties	Upstroke velocity	~50 V/s	~50 V/s	~250 V/s	*33,40*
	Synchronous contraction	No	No	Yes	*41*
	Resting membrane potential	~-60 mv	~-60 mv	~-90 mv	*12*

2.3) Current maturation strategies

Previous study demonstrated that maturation of PSC-CMs arrested at late-embryonic cardiomyocytes after long-term culture *in vitro*[1]. In contrast, PSC-CMs underwent structural and functional maturation for one-two months when transplanted into a neonatal rat heart *in vivo*[42]. These results indicated that PSC-CMs could mature if appropriate environments are provided. Interestingly, even human PSC-CMs could mature with the *in vivo* maturation method for two months, although human CMs require more than five years of maturation in the human heart (Fig. **3**). Subsequently, there are numerous efforts that mimicked microenvironment during heart development to enhance the maturation of PSC-CMs such as long-term culture, cultured on ECMs, postnatal hormone treatments, adjusting substrate stiffness, electrical stimulation, as well as co-culture with non-CMs (Fig. **4**). These maturation strategies are described below.

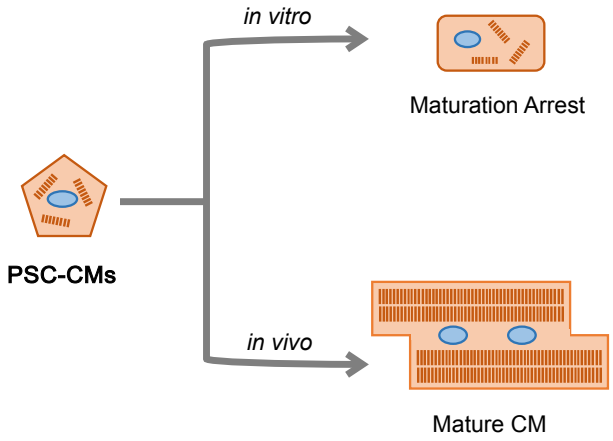

Figure 3. PSC-CMs can be matured *in vivo* but not *in vitro*.

2.3.1) Long-term culture

Fundamentally, CM maturation is a gradual process that requires long time. Indeed, human neonatal CMs develop their adult phenotype about 6-10 years *in vivo*[43], while beating human and mouse PSC-CMs are generated within only 7 days of differentiation[1,44]. To imitate the maturation process, PSC-CMs are initially increased the time for culture in a dish (Fig. **4a**). Lundy *et al* showed that culturing human PSC-CMs up to 120 days resulted in morphological changes towards adult-like mature CMs including an increase in sarcomere length, cell size, elongated shape, as we as binucleation[33]. Moreover, sarcomere organization study demonstrated that Z and I

bands have appeared after culture the PSC-CMs for 30 days. Then, extended culture for 30-90 days resulted in A-bands development, followed by induction of M-bands formation after culture up to 360 days[45]. Along with the electrophysiological study, transient outward and inward rectifier potassium currents (I_{to1} and I_{k1}) were increased through a prolonged culture[46]. Although long-term culture of PSC-CMs enhances several aspects of CM maturation as mentioned above, it is still a low-throughput and time-consuming method. To accelerate CM maturation, diverse maturation strategies have emerged.

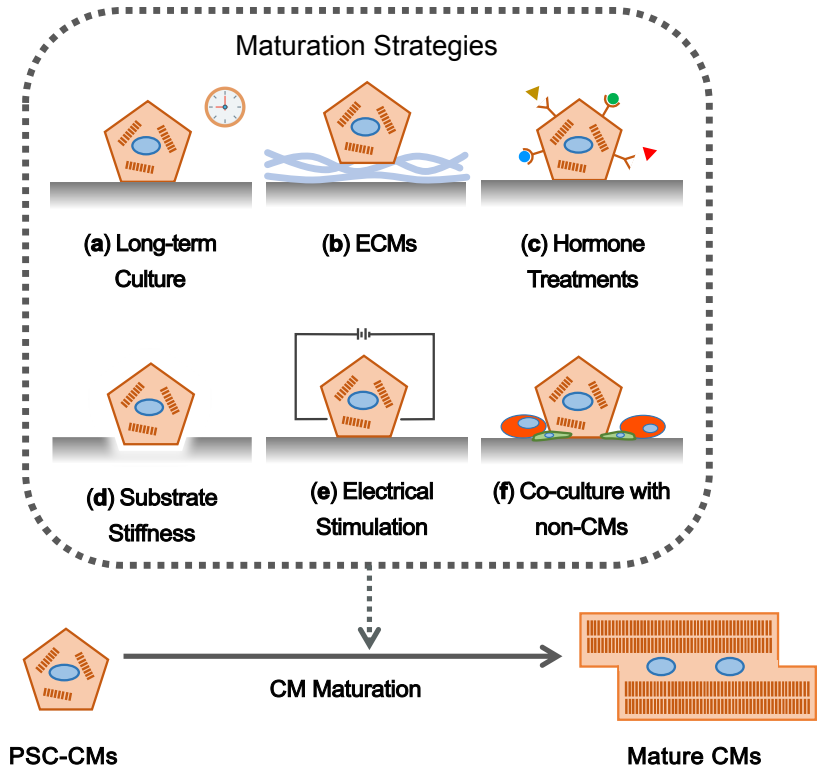

Figure 4. Current strategies for promoting cardiomyocyte maturation.
To enhance CM maturation, several strategies have been developed such as (**a**) long-term culture, (**b**) ECMs, (**c**) hormones, (**d**) substrate stiffness, (**e**) electrical stimulation, and (**f**) co-culture with non-CMs.

2.3.2) Extracellular matrices

ECMs do not only provide structural support during heart development, but also contain signaling molecules for transmitting signals between CMs and neighboring tissues[47]. Thus, ECM substrates are required for CM maturation (Fig. **4b**). Previous study has shown that PSC-CMs cultured on cardiogel, containing cardiac fibroblast, laminin, fibronectin, collagen type I and III, and proteoglycans, exhibited more mature

phenotypes such as spontaneous contractility, hypertrophy and cytoskeleton differentiation faster than 2-dimensional culture system[48]. Consistently, culturing PSC-CMs on overlaid matrigel consisted of laminin, collagen type IV, and proteoglycan improved electrophysiological properties of the treated PSC-CMs[49]. These results raise the important roles of ECMs on CM maturation.

2.3.3) Hormones

Postnatal hormones are considered as one of the enhancers for CM maturation (Fig. **4c**). Specifically, treating PSC-CMs with triiodothyronine (T3) has been shown to increase cell size and elongation, contractility, and sarcomere length compared to non-treatment[50]. Furthermore, T3 treatment was also shown to be effect for several cardiac gene expressions such as *α-MHC*, titin, and *SERCA2a*[50,51]. T3 even showed a significant increase in mitochondrial activity both maximal respiratory capacity and respiratory reserve capacity[50]. In addition to T3 treatment, PSC-CMs treated with dexamethasone, a synthetic glucocorticoid, showed significantly faster calcium decay, increased forces of contraction, and sarcomere length[52]. A combination of T3 and dexamethasone applied to PSC-CMs also induced T-tubule formation and increased excitation-contraction coupling[53]. These results provide important evidence that hormones are essential for CM maturation.

2.3.4) Substrate stiffness

Spatial change of microenvironment generally occurs during heart development, for instance, a collagen accumulation in mice heart. This change combined with other dynamic changes results in a 3-fold increase of myocardium elasticity from embryo to neonatal stage[54], and a 2-fold increase from neonatal to adult heart[55] (Table **2**). Coincidentally, this process appears postnatally with the elevation of blood pressure and the capability of pumping blood by the heart. Therefore, substrate stiffness is one of the microenvironments that has been widely investigated their effect on CM maturation (Fig. **4d**). Previous study found that CMs are well developed on the optimal substrate of comparable stiffness to that of native tissue[56] (Table **2**). Consistently, Jacot *et al* also demonstrated that neonatal rat ventricular heart myocytes (NRVM) plated on collagen-coated polyacrylamide with substrate stiffness similar to native myocardium, 10 kPa, appeared aligned sarcomere better than stiffer or softer substrates. The treated-cells were generated greater mechanical force, had the

highest calcium transients, and increased *SERCA2a* expression, on 10 kPa gel[57]. Altogether, substrate stiffness effects to physical and functional maturation of CMs.

Table 2. Elasticity of different types of myocardial tissue.

Myocardium Type	Elasticity	Elasticity Change	Ref.
Neonatal rat	4.0-11.4 kPa	3-fold	54,58–60
Adult rat	11.9-70 kPa	2-fold	55,58–61
Adult human	0.02-0.5 MPa	-	62

2.3.5) Electrical stimulation

CMs are constantly subjected to electrical impulses conferring spontaneous rhythmic contraction. Thus, electrical stimulation has been expected to promote CM maturation (Fig. **4e**). Interestingly, a transcriptome analysis of rat CMs found that known cardiac-specific genes such as *MYH6*, *Cx43*, and L-type calcium channel (*CACNA1C*), were highly upregulated following electrical stimulation. Moreover, NRVM in collagen sponges were increased contraction amplitude and improved their alignment after applying electrical stimulation[63]. Stimulation of NRVM monolayer was also increased several maturation aspects of CMs including sodium-calcium exchanger, action potential duration, conduction velocity, and even mitochondrial activity[64,65]. Although electrical stimulation has impacted CM maturation, it has known a little and usually combined with other maturation strategies[66]. Thus, several confounding factors such as ECM interaction, may result in interference with the effects of electrical stimulation[67].

2.3.6) Co-culture with non-CMs

Rat heart consists of 30% CMs, 6% endothelial cells (ECs), and 64% fibroblasts (FBs)[68]. During heart development, CMs interact closely with other cell types. Thus, non-CMs can contribute to CM maturation *in vivo* either cell-to-cell contact and paracrine effects[30] (Fig. **4f**). The imitation of the cardiac microenvironment is important for cardiac differentiation and also maturation. Previous study showed that non-CMs are necessary for the development of intracellular calcium handling proteins, ion channel development and electrophysiological maturation of human ESC-CMs[69]. Additionally, co-cultured immature CMs with ECs and/or FBs seems to exert an effect to CM maturation after engraftment to the animal models. Recent study by Gao *et al*,

who generated human cardiac muscle patches (hCMPs) consisting of CMs, smooth muscles, and ECs differentiated from human iPSCs, showed that hCMPs were improved electronic mechanical coupling, calcium handling, and force generation after 7 days of dynamic culture *in vitro*[70]. Co-culture with other cell types not only effected functional improvement of CMs *in vitro*, but also achieved in clinical relevance when engrafted to animal myocardial infraction models (MI)[70].

Individual maturation strategies are able to improve many aspects of CM maturation. But it is insufficient to generate fully mature CMs. Recently, combinations of several available strategies have been incrementally used to generate more mature PSC-CMs. For example, the combination of electrical and mechanical stimulations showed an increase in 2-fold of contractile forced[71]. Moreover, 3-dimensional (3D) engineering of heart tissues with other cell types and combined with ECMs enhanced morphological and functional maturation. Previous studies also demonstrated that 3D cardiac patches using modified substrates and co-culture with non-CMs not only improved morphology and function of PSC-CMs, but also achieved in a clinical trial when engrafted the PSC-CMs to animal MI models[70,72]. Although combinations of maturation methods are documented, the maturity of PSC-CMs with those manners compared to *in vivo* CMs remains unknown and no assessment tool is available.

2.4) Assessment methods for CM maturation

Since maturation strategies have been developed and applied to PSC-CMs in order to enhance their maturity towards adults-like CMs, morphological and functional assays are extensively used as assessment tools for CM maturation. For instance, immunostaining is used to determine the ultrastructure of those CMs such as sarcomere structure and cell morphology[73]. Transcriptome analysis is conducted to examine entire gene expressions following tested condition[1]. Action potential and calcium transients are assays that used to determine physiological properties of CMs, due to adult CMs have orchestrated activity among several ionic channels, conferring particular patterns of action potential and calcium transients[13,74]. In addition, contractile forces are also one of the parameters that are used to compare maturity between immature and mature CMs[75]. Moreover, mitochondrial activity is also conducted to examine responsibility for the energy-generating process based on metabolic switches from glycolysis to fatty acid metabolism during heart

development[76]. Although these assays are able to determine how maturation strategies improve PSC-CMs maturation, the assays are varied from lab-to-lab, time consumptions, and unable to determine the exact maturation status of PSC-CMs under those maturation strategies. To date, there is no potential high-throughput method that is able to assess the exact maturation degree of PSC-CMs. Thus, my ultimate goals are to generate fully matured CMs through developing novel qualitative and quantitative methods for determining CM maturation on ECMs.

For the qualitative method, fluorescent reporters have been widely used to understand and improve differentiation of a certain cell type or lineage in developmental biology and stem cell biology[77]. Thus, I hypothesized that a novel fluorescent reporter line would help me to determine the maturation state of PSC-CMs easily and rapidly. Here, I developed a novel fluorescent reporter line, using Myom2 gene as a candidate maker of CM maturation. For the quantitative method, I collected a reference transcriptome dataset from embryos to adults with a cost-effective transcriptome method using Quant-seq, 3'mRNA sequencing. Next, I compared the transcriptome of the treated PSC-CMs to mouse heart counterparts and quantitatively assessed the maturation status according to the microarray-based method as shown in the previous paper[1]. I believe that the novel maturation reporter will unlock the promising benefits of using PSC-CMs in advanced medical applications.

Chapter 3
Methods

3.1) Mouse ESCs (mESCs) maintenance

mESCs were used in this research including syNP4[78], and fluorescence maturation reporter lines (SMM18, and SMMB2). These cells were cultured in 0.1% (w/v) gelatin-coated tissue culture plates without feeders in 2i medium[79] containing particular components as described in Table **3**. These cell lines were cultured at 37 °C humidified air with 5% CO_2, and passaged every 2-3 days.

Table 3. 2i medium for moue ESCs maintenance.

Component	Company	Amount/Concentration
Glasgow minimum essential medium (GMEM)	Sigma	450 ml
Fetal bovine serum (FBS)	Moregate	10% (50 ml)
Leukemia inhibitory factor (LIF)	ESGRO	1,000 U/ml
2-mercaptoethanol	Thermo Fisher Scientific	0.1 mM
CHIR99021	Stemcell Technologies	3 μM
PD0325901	Stemcell Technologies	1 μM
Glutamax	Thermo Fisher Scientific	2 mM
Sodium pyruvate	Thermo Fisher Scientific	1 mM
MEM non-essential amino acids (100x)	Thermo Fisher Scientific	Diluted to 1x

3.2) Cardiomyocyte differentiation

Cardiac differentiation was performed in accordance with our previous report[1]. In brief, serum-free differentiated medium (SFD)[80] was used as a basal medium. The specific ingredients for SFD medium are explained in Table **4**. SMM18 or SMMB2 was suspended culture in SFD medium for 2 days, before mesodermal induction. Then, medium was changed with 5 ng/ml activin-A (R&D System), 1.9 ng/ml bone morphogenetic protein 4 (BMP4, R&D System), and 5 ng/ml vascular endothelial growth factor (VEGF, Wako) and cultured cells for more additional 2 days. At day 4, the cells were plated and induced to cardiac progenitors through the addition of 5 ng/ml

VEGF, 10 ng/ml basic fibroblast growth factor (bFGF, R&D System), and 25 ng/ml FGF10 (R&D System). Until day 7, fresh SFD medium containing puromycin was replaced to enrich CMs. To determine the purity of CMs, cells were immunolabeled with cardiac troponin T (cTnT, a cardiac marker), and then performed flow cytometry as depicted in Method **3.6**. With the antibiotic selection, more than 90% of PSC-CMs were obtained. These high purity CMs were used to run all of the experiments. For long-term culture, I plated the cells at day 10 and cultured in SFD medium up to day 38. For the remained PSC-CMs, I preserved the cells in liquid nitrogen using a freezing medium containing 70% IMDM, 20% FBS, and 10% Dimethyl sulfoxide.

Table 4. SFD medium for cardiac differentiation and PSC-CMs maintenance.

Component	Company	Amount/Concentration
Iscove's modified Dulbecco's medium (IMDM)	Thermo Fisher Scientific	375 ml
Ham's F12 medium	Thermo Fisher Scientific	125 ml
B27 without retinoic acid (50x)	Thermo Fisher Scientific	Diluted to 0.5x
N2 supplement (100x)	Thermo Fisher Scientific	Diluted to 0.5x
Bovine Serum albumin	Sigma	0.05% (w/v)
Glutamax	Thermo Fisher Scientific	2 mM
Ascorbic acid	Wako	0.05 mg/ml
1-thioglycerol	Sigma	450 μM

3.3) Generation of Myom2-RFP reporter line

Here, I designed a single-guide RNA (sgRNA), which targets to 3' end of *Myom2* gene, and cloned to px330 as explained in previous work[81]. The sgRNA sequence is showed in Table **5**. The three nucleotides labeled with red color (TAA) are stop codon of *Myom2* gene. TagRFP and blasticidin-resistance cassette were inserted to the stop codon of *Myom2* and PAM sequence (Fig. **10a-i**). TagRFP was designed to be in-frame to endogenous *Myom2*. px330 with Myom2 sgRNA and the targeting vector were co-transfected to syNP4 cells, parental mESCs (Fig. **10a-ii**). Then, I screened blasticidin-resistant clones using PCR with the primer combinations including 5F2/TR and Blast/Downstream (Fig. **10-iii**). Sequencing was used to confirm

site-specific integration. For the clones that achieved targeting integration, I called them as SMM clones (Fig. **10b**). Then, I further examined cardiac differentiation efficiency and RFP expression in the prolonged culture of those SMM clones. The clone which could differentiate into CMs in high yield and express RFP, was then selected and remove the blasticidin-resistance cassette by transfecting with CAG-Flpe-IRES-Puro (Fig. **10a-iv**). Short-term treatment of puromycin (for one day) was conducted to enrich transfected cells. Removing the blasticidin-resistance cassette was confirmed by PCR with primer sets of 3F1/Downstream and Blast/Downstream. The clones that were depleted blasticidin-resistance cassette are called as SMMB clones (Fig. **10b**). After that, I also confirmed blasticidin and puromycin sensitivities of the SMMB clones in undifferentiated stage. I again confirmed the clones that were able to differentiate well into puromycin-resistant CMs and RFP expression after prolonged culture. All of the primer sequences were used in fluorescence reporter generation are listed in Table **5**.

Table 5. sgRNA and primers for generation of Myom2-RFP reporter lines.

Name	Direction	Sequence (5' to 3')
sgRNA	-	GCTTCCACCTCATCTGATTA+AGG
5F2	Forward	GTCACAGGGACATAGGCACTT
TR	Reverse	GATGTGCACTTGAAGTGGTG
Blast	Forward	AAAAGCCTCCTCACTACTTCTGG
Downstream	Reverse	GAAGGGTACTTAACCCAGGAACC
3F1	Forward	GAGGACTCGGGCAAGTACAG

3.4) Flow cytometry

For checking %cTnT of cardiac differentiation, SMM18 or SMMB2 was differentiated by following the differentiation protocol until day 10 (Method **3.2**). Then, the cells were dissociated and fixed with 4% (w/v) paraformaldehyde (PFA, Wako). Cells were permeabilized and blocked with 0.2% Triton X-100 containing 5% FBS in phosphate-buffered saline (PBS). Following this step, anti-cTnT monoclonal antibody (13-11, 1:500, Thermo Fisher Scientific) was used to stained the cells for 30 minutes at room temperature. After that, cells were washed and stained with secondary antibody, anti-mouse IgG conjugated with Alexa Fluor 488 (1:500, Thermo Fisher

Scientific). DAPI solution (Dojindo Laboratories) was used for labeling DNA in the nucleus. Measurement of %cTnT was conducted by SH800 (SONY).

For quantifications of Myom2-RFP$^+$ cells and RFP intensity, cells were cultured until the desired time. After cell dissociation, the cells were washed with PBS and sequentially suspended with 2% FBS in PBS containing DAPI solution (1:2000) to discriminate death and live cell populations. Similar to %cTnT, measurements of the proportion of RFP$^+$ cells and RFP intensity were performed using SH800 (SONY).

3.5) RNA sequencing

The PSC-CMs at different time points of cardiac differentiation and mouse hearts (E11 to 10 months postnatal, 10M) were collected and extracted RNA according to the manufacturer's protocol for Direct-zol RNA extraction kit (Zymo Research. Qubit 4 Fluorometer (Thermo Fisher Scientific) was used to quantify the amount of RNA from each sample. cDNA was prepared by Quant-seq 3' mRNA-Seq library prep kit FWD for Illumina (Lexogen) according to the manufacturer's protocol using approximately 500 ng of total RNA per sample. Library concentrations and size-distribution were then confirmed by Qubit 4 Fluorometer and Agilent 2100 Bioanalyzer (Agilent Technologies), respectively. cDNA library was pooled from each cDNA sample and sequenced by the Illumina NextSeq (75 cycles, single-end). Adapter and quality trimming was performed with BBDuk, then the trimmed reads were mapped to the GRCm38 mouse genome using STAR RNA-seq aligner[82]. To count the mapped read, featureCounts was used[83]. The read counts were normalized to transcript per million to show gene expression levels and/or compare expression levels between genes. To compare expression levels between samples, the read counts were normalized to regularized log (rlog) using DEseq2[84]. To perform GO analysis, enrichGO function in clusterProfiler was used[85].

Using the transcriptome data, I also performed a principal component analysis (PCA) and calculated the maturation score of each sample. To this end, I have set a weight for each gene in principle component 1 (PC1) axis. The maturation score is a summation of expression levels of each gene (transcript per million reads, TPM) multiplied by the weight for PC1 as shown in the formula below.

$$\text{Maturation Score} = k(\Sigma\ \boldsymbol{\varepsilon_i}\ \boldsymbol{\omega_i} + \text{Offset})$$

$\boldsymbol{\varepsilon_i}$ is expression of i gene

$\boldsymbol{\omega_i}$ is weight of i gene

k is a constant to make the maturation score ranging from 0-100

Offset is a constant to make score > 0

3.6) Immunostaining

To conduct immunostaining for hearts, I collected the heart tissues from different stages of developing mouse including E16.5, postnatal day 4 (P4), and adult. The hearts were embedded in optimal cutting temperature (OCT) compound (Tissue-Tek, Sakura) and directly frozen in liquid nitrogen. The heart tissues were cut into several thin layers around 4 μm using Leica Cryostat. Then, heart tissues were fixed in 4% (w/v) PFA, for 30 minutes at 4°C. The sections were washed and permeabilized using 0.1% Triton X-100 (Amersham Biosciences) in PBS for 15 minutes at room temperature. After permeabilization, non-specific binding sites were saturated by incubation with 3% bovine serum albumin. Primary antibodies were anti-Myom2 (LS-B9842, 1:100, LifeSpan BioSciences) and anti-α-actinin (EA-53, 1:100, Sigma-Aldrich). Anti-rabbit IgG conjugated with Alexa Fluor Plus 555 (1:500, Thermo Fisher Scientific) and anti-mouse IgG conjugated with Alexa Fluor Plus 488 (1:500, Thermo Fisher Scientific) were used to reveal primary antibody signals. Nuclei were stained with DAPI (1:2000) and slides were mounted in VECTASHIELD Antifade Mounting Medium (Vector Laboratories). A confocal laser scanning microscope (Olympus FluoView FV1200) was used to obtained immunofluorescence images.

To perform immunostaining for PSC-CMs, the monolayer cells cultured in CellCarrier 96-well black polystyrene microplate (PerkinElmer) were fixed with 4% (w/v) PFA for 30 minutes at room temperature. Then, the cells were washed with PBS and permeabilized using 0.2% Triton X-100 in PBS for 15 minutes at room temperature. After that, blocking was conducted using 2% FBS in PBS. To perform immunolabeling, cells were incubated with primary antibodies including anti-α-actinin antibody (1:500) or anti-cardiac troponin T antibody (1:500), and anti-tRFP (AB233, 1:500, Evrogen) for overnight. Following this step, the cells were washed with PBS to remove excess primary antibodies and incubated with secondary antibodies such as anti-mouse IgG conjugated with Alexa Fluor 488 (1:500, Thermo Fisher Scientific) and anti-rabbit IgG

conjugated with Alexa Fluor 555 (1:500, Thermo Fisher Scientific). Nuclei were stained with DAPI (1:2000). An inverted fluorescence microscope (Olympus IX83) was used to obtained immunofluorescence images. Cell morphological parameters including sarcomere length, cell size, circularity, perimeter, as well as cell geometry (length and width), were analyzed by ImageJ software.

3.7) Calcium transients and sarcomere shortening assay

Evaluation of intracellular calcium transients was carried out using live-cell imaging analysis. Briefly, cells were plated on glass bottom 24-well plates (MatTek Corporation) until the desired day to run the experiment. Then, cells on the glass bottom plates were washed with PBS and incubated with 5 μM Calbryte 520-AM (AAT Bioquest), intracellular calcium-sensitive dye, in freshly prepared Tyrode's solution (Table **6**), for 30 minutes at room temperature. Cells were evoked by electrical field stimulation at 1 Hz (C-Pace, IonOptics). Optical recordings of intracellular calcium transients were acquired using an inverted fluorescence microscope (Olympus IX83 with ORCA-Flash4.0 V3) with a 40x objective lens, 10 msec exposure and 20 msec interval. The optical records were then analyzed by ImageJ software as described in previous report[86]. For sarcomere shortening, cell contraction was recorded continuously with time-lapse videos for live-cell imaging. The time-lapse recordings were then analyzed by SarcOptiM for ImageJ as explained in the previous study[87].

Table 6. Components of Tyrode's solution.

Component	Company	Concentration
NaCl	Wako	140 mM
KCl	Wako	5.4 mM
$MgCl_2$	Wako	0.5 mM
NaH_2PO_4	Wako	0.33 mM
$CaCl_2$	Wako	2 mM
HEPES	Dojindo	5 mM
D-Glucose	Wako	11 mM
pH adjusted to 7.4 with NaOH		

3.8) Mitochondrial activity assay

PSC-CMs were seeded on an ECM-coated XFe96 Cell Culture Microplate (Seahorse Bioscience) at $5x10^4$ cells/well, and prolonged culture up to day 38. Oxygen consumption rate (OCR) was measured by an Agilent Seahorse XFe96 Extracellular Flux Analyzer (Seahorse Bioscience) in XF RPMI medium supplemented with 1 mM pyruvate, 2 mM glutamate and 25 mM glucose. OCR was measured before and after the sequential addition of 3 μM oligomycin, 0.5 μM carbonyl cyanide-4 (trifluoromethoxy) phenylhydrazone (FCCP), and 3 μM rotenone/antimycin A. Basal respiration was represented by OCR rate before applying oligomycin. ATP-linked respiration was represented by the oligomycin-sensitivity respiration rate, while proton leak was calculated by the difference between oligomycin and rotenone/antimycin rates. Maximal mitochondrial respiration was the response to FCCP.

3.9) Statistical analysis

Data are presented as mean ± standard deviation (SD) for at least three replicate samples. Student's *t*-test, Dennett's test, chi-square test, or one-way ANOVA were used to determine whether any statistically significant difference exists among independent groups, as described in legends. All of the statistical analysis was performed using R statistical software. A *p*-value of less than 0.05 was considered to have statistical significance.

Chapter 4

Results

4.1) Cardiac differentiation

CMs could be efficiently obtained from mESCs through cardiac differentiation *in vitro*[9]. The differentiation protocol was described in Method **3.2** and a schematic protocol was shown in Fig. **5a**. Briefly, mESCs were cultured as a suspension in SFD medium for 2 days before mesodermal induction. Then, medium was changed with SFD supplemented with activin-A, BMP4, and VEGF for 2 more days. After day 2 to day 4, embryoid bodies were formed (Fig. **5b**). Cells were then subjected to trypsinization and cultured with the sequential addition of bFGF, FGF10, and VEGF, to induce cells towards cardiac lineage. Until day 7 of differentiation, fresh SFD medium was replaced. At this time point, the cells started to beat, hereafter called "PSC-CMs". To determine the amount of PSC-CMs, cells were immunolabeled with cTnT and performed flow cytometry at day 10 of differentiation (Fig. **5a-b**).

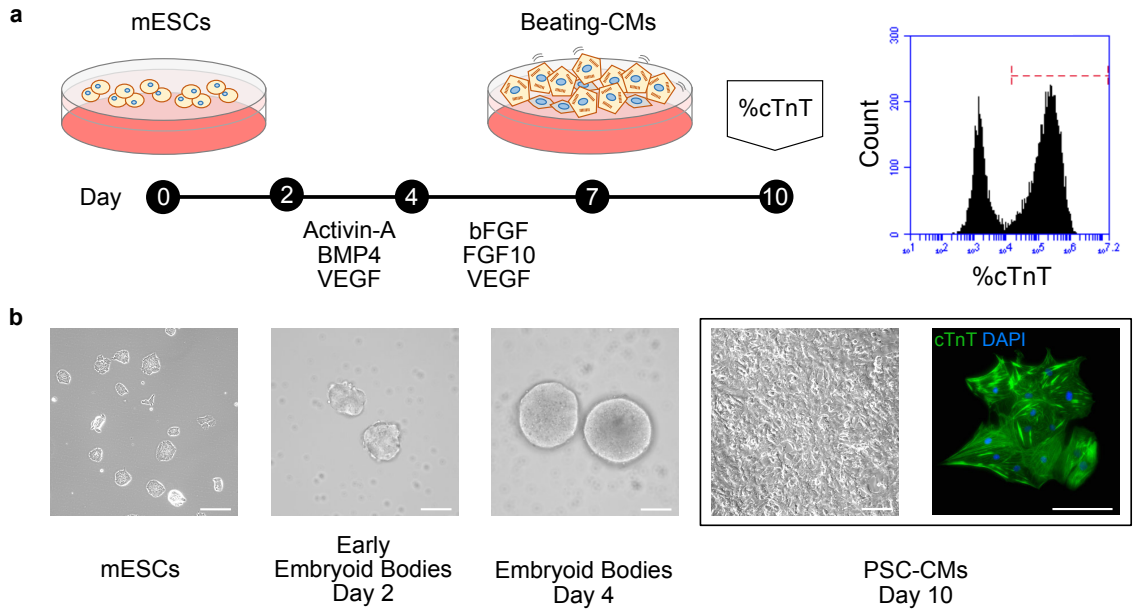

Figure 5. Differentiation protocol for obtaining CMs from mESCs

(**a**) Timeline diagram demonstrating the cytokines that were used for mESCs differentiation. After 10 days of differentiation, flow cytometry for cardiac troponin T (cTnT, a marker for CMs) was performed to determine the purity of PSC-CMs. (**b**) Cell morphology of mESCs, embryoid bodies at day 2 and 4, as well as PSC-CMs at day 10 of cardiac differentiation. Scale bar = 50 μm.

4.1.1) BMP4 induces cardiac marker protein expressions

The concentration of BMP4 is known that critical for mesodermal induction in serum-free medium[80,88,89]. Therefore, I differentiated mESCs towards CMs by which titration BMP4 concentration ranging from 0.25 to 1.5 ng/ml, to determine the effect of BMP4 for cardiac differentiation (Fig. **6**). After day 10, PSC-CMs were stained with α-actinin and cTnT to examine the expressions of those cardiac makers. The result illustrated that BMP4 was promoted both α-actinin and cTnT expressions as dose-dependent manners (Fig. **6a-b**). Those marker proteins were initially expressed in the condition of 1 ng/ml BMP4. To determine the percent of $cTnT^+$ cells, flow cytometry was performed. In agreement with immunostaining results, the percent of $cTnT^+$ cells were gradually increased from low to high BMP4 concentration, suggesting the important role of BMP4 for cardiac differentiation (Fig. **6c**).

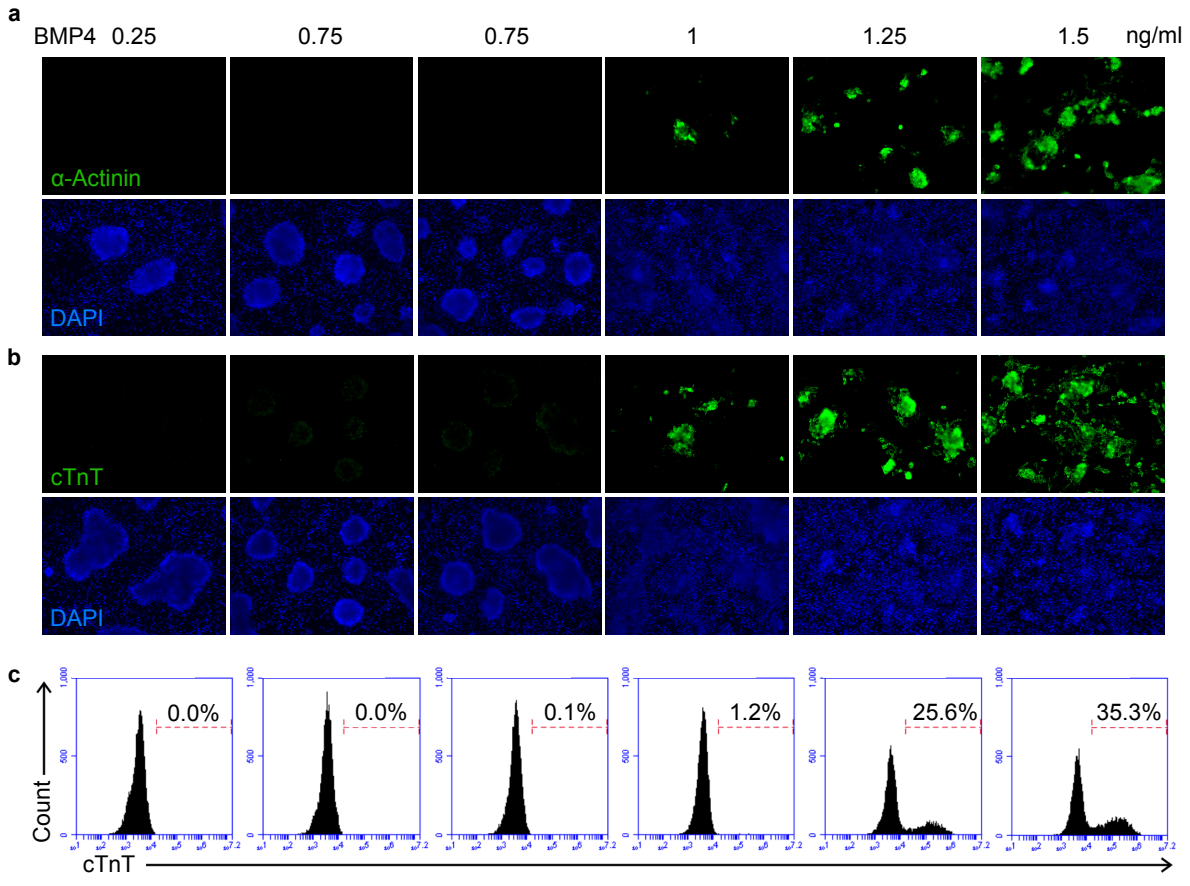

Figure 6. Important role of BMP4 for cardiac differentiation.
Immunostaining for cardiac marker expressions including α-actinin (**a**) and cTnT (**b**), after varying BMP4 concentration. (**c**) Quantification of cTnT expression with indicated BMP4 concentration at day 10 of cardiac differentiation.

4.1.2) Optimization for cardiac differentiation and PSC-CMs enrichment

Cardiac differentiation was optimized by varying the concentration of BMP4, ranging from 1.5 to 2.5 ng/ml. The mESCs were used to titrate BMP4 concentration including a parental cell line (syNP4) and Myom2-RFP reporter line (SMM18 and SMMB2). Cardiac differentiation efficiency was evaluated as the percentage of cTnT-expressing cells at day 10 of differentiation. The result found that at 1.9 ng/ml BMP4 showed the highest percent of $cTnT^+$ cells approximately 60-70% in all of the tested mESCs (Fig. **7a**). To further enrich PSC-CMs, I used syNP4 as a parental mESC line. This cell line has a puromycin resistance cassette driven by sodium-calcium exchanger 1 (NCX1) promoter which is only active in CMs, but not in non-CMs. Therefore, I could remove other cell types from the culturing system by puromycin selection (Fig. **7b**). With optimal BMP4 and antibiotic selection, more than 90% of $cTnT^+$ cells were obtained from this differentiation system (Fig. **7c**).

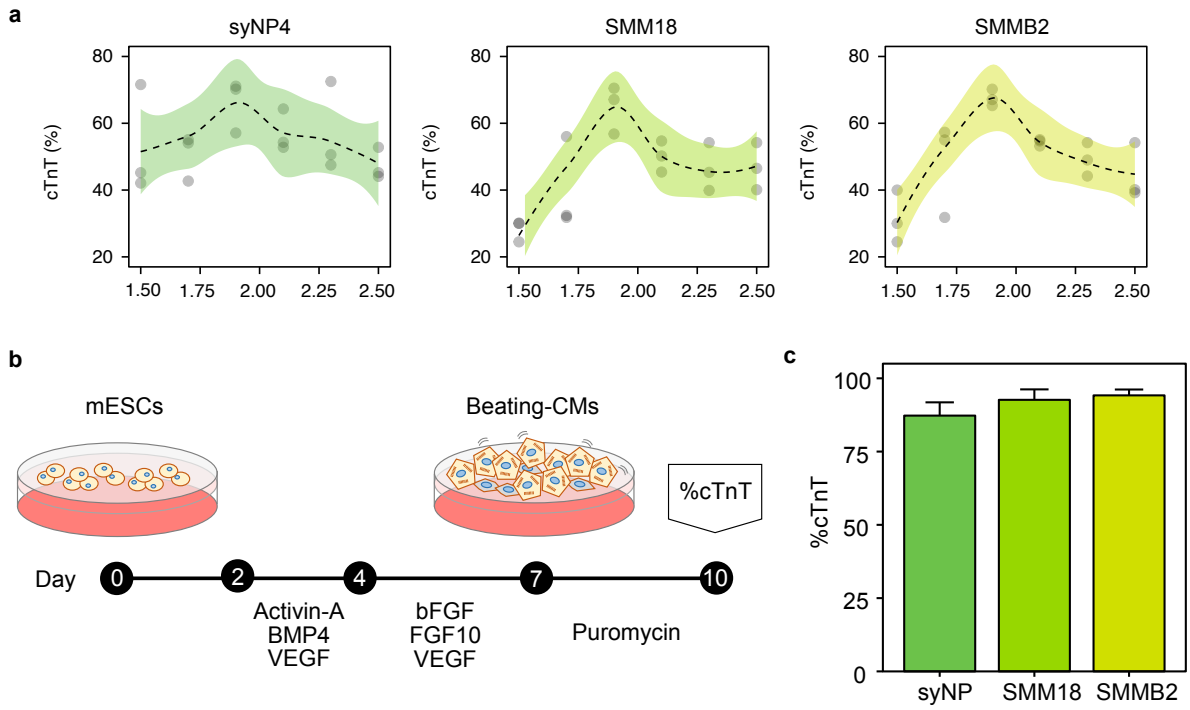

Figure 7. Optimization for cardiac differentiation and enrichment.

(**a**) Optimization of BMP4 concentration (ranging from 1.5 to 2.5 ng/ml) for cardiac differentiation of mESCs including syNP4, SMM18, and SMMB2. Data were shown as scatterplots with smooth fitted lines (n = 3). (**b**) Schematic representation of cardiac differentiation from mESCs using the sequential addition of cytokines followed by enrichment with puromycin. (**c**) Validation of the optimal condition (1.9 ng/ml BMP4 and puromycin selection) with mESCs. Data are presented as means ± SD (n > 4).

4.2) Generation of a fluorescent reporter line for CM maturation

4.2.1) Myom2 is selected as a reporter

To determine candidate genes for CM maturation, I examined gene expression profiles during heart development (E11 to P56). I identified 11 candidate genes including *Atp1a2*, *Ckmt2*, *Cox7a1*, *Gsn*, *Hspb8*, *Myom2*, *Myoz2*, *Rpl3l*, *s100a1*, *Tcap*, and *Xirp2*, using two criteria; (1) at least 2-log fold change at one point between E16-P1, P1-P7, P7-P14 and neonate (P1-P7) to adult (P14-P56), and (2) at least 500 transcripts per million reads (TPMs) at P56 to ensure that the expression levels would be much enough and able to detect for reporter signal (Fig. **8**).

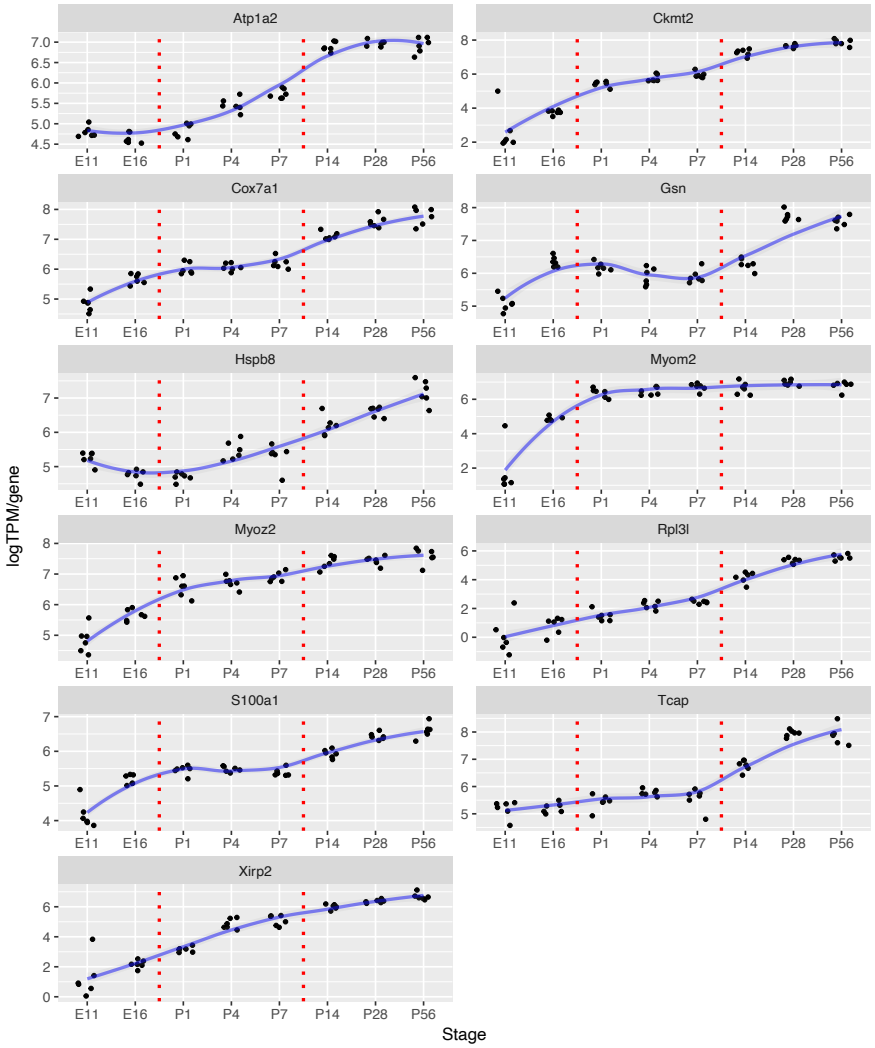

Figure 8. Expression profiles of candidate genes for CM maturation.
The candidate makers for CM maturation that were selected in this study consist of 11 genes, including *Atp1a2*, *Ckmt2*, *Cox7a1*, *Gsn*, *Hspb8*, *Myom2*, *Myoz2*, *Rpl3l*, *s100a1*, *Tcap*, and *Xirp2*. TPM, transcriptome per million reads.

Among the candidate genes, *Myom2* not only showed earlier expression than the others, but its expression also gradually increased up to adult stage (Fig. **8** and Fig. **9a**). To generate a fluorescent reporter, the expression of the reporter gene conferring fluorescence signal to visible level, is required. Therefore, *Myom2* was selected as a reporter gene in this study.

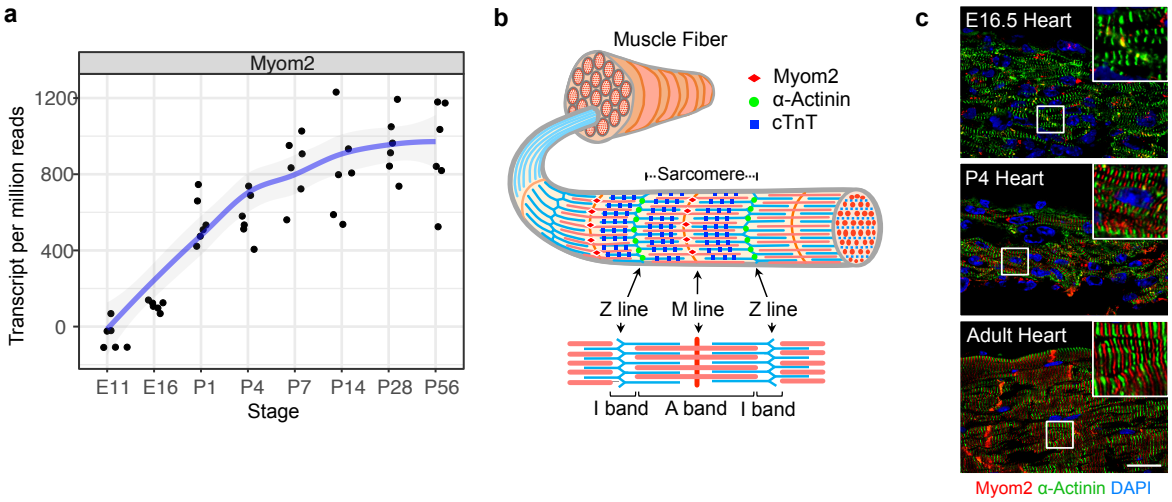

Figure 9. Myom2 expression profile and its localization in the mouse heart.
(**a**) Expression profile of Myom2 during heart development from mouse E11 to P56. RNA expression level was presented as transcriptome per million reads. Data were shown as a scatterplot with a smooth fitted line (blue line), called Locally Weighted Scatterplot Smoothing (LOWESS). (**b**) A schematic demonstrating localizations of Myom2 (red), α-actinin (green), and cTnT (blue), in sarcomeres. Myom2 is encoded to M-protein which locates in the M-line of the sarcomere structure, whereas α-actinin is in Z-line. Therefore, Myom2-RFP would be observed in between Z-lines of the sarcomeres. (**c**) Representative images for Myom2 expression and localization in developing mouse hearts. Scale bar = 20 μm. These images are modified from data submitted to *Sci Rep*.

Myom2 is encoded to M-protein that localized to M-lines of the sarcomeres[90–92] (Fig. **9b, 9c**). To generate a fluorescence maturation reporter, I inserted sequence encoding the RFP into the genomic locus of Myom2 in syNP4 cell line. For the reason to use syNP4 as a parental cell line is that Myom2 is not only expressed in cardiac muscle, but also found in skeletal muscle[93]. Thus, using syNP4 cells will allow us to select CMs by puromycin treatment as mentioned before (Result 4.1.2). To achieve

knock-in efficiency, I used CRISPR/Cas9 system to generate double strand break at the target region (Fig. **10a**). syNP4 cells were co-transfected with a vector expressing Cas9 and single-guide RNA and a targeting construct. After blasticidin selection, the insertion of TagRFP into *Myom2* genomic locus was confirmed using PCR screening (Method **3.3**). Several subclones including SMM2, 18, 19, and 23, were identified as inserted TagRFP (Fig. **10b**, top panel). After confirming that SMM18 differentiated to CMs similarly to the parental line (syNP4), the blasticidin-resistance cassette was removed from SMM18 using flippase site-specific recombination (Fig. **10a**). Excision of the blasticidin-resistance cassette were confirmed in SMMB1, 2, 5, 6, and 7 (Fig. **10b**, bottom panel) by PCR screening (Method **3.3**). Among these subclones, SMMB2 and 5 were differentiated to PSC-CMs well. Therefore, SMM18 and SMMB2 were used to run all of the experiments in this study.

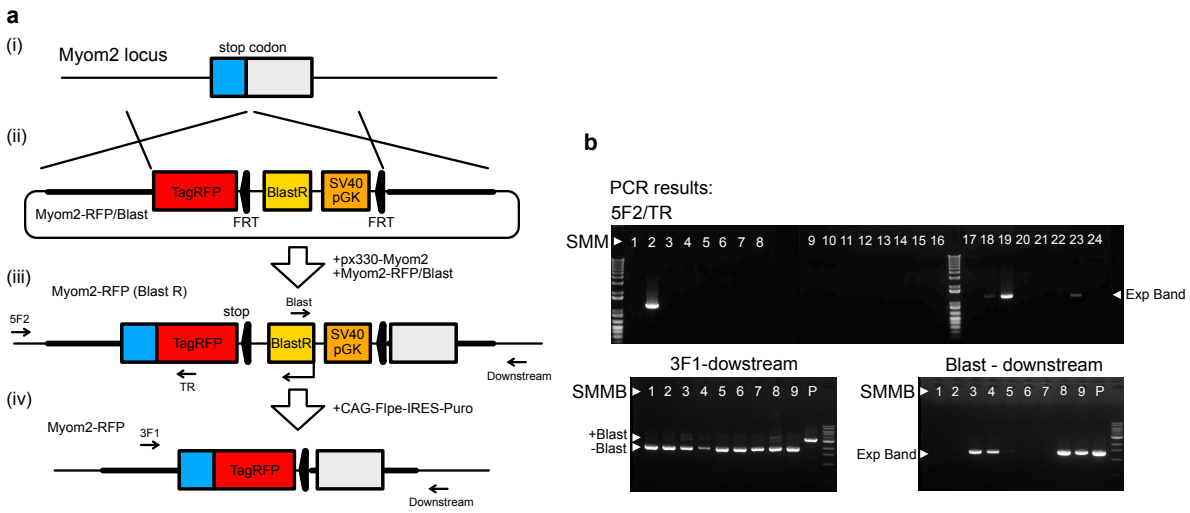

Figure 10. Knocking-in RFP into 3' endogenous of Myom2.

(**a**) Schematic image for the generation of Myom2-RFP reporter; (i) stop codon of Myom2, (ii) Myom2-RFP/Blast targeting construct, and the resulting targeted (iii) with and (iv) without blasticidin resistance cassette. Forward and reverse primer binding regions for PCR screening are also shown in the image. (**b**) PCR screen to identify targeted clones. The upper panel shows 3' end screen of integration of TagRFP in subclones SMM2, 18, 19, and 23. The lower panel presents confirmation of excision of the blasticidin-resistance cassette in subclones SMMB1, 2, 5, 6, and 7. These images are modified from data submitted to *Sci Rep*.

4.2.2) Myom2-RFP is exclusively localized to M-lines of the sarcomeres

As Myom2 localizes to M-lines of the sarcomeres, Myom2-RFP was expected to appear in between Z-lines which are α-actinin regions. To this end, I next determined the localization of Myom2-RFP that appeared in PSC-CMs by immunostaining (Fig. **11**). Consistent with this idea, the results demonstrated that Myom2-RFP expression showed an alter pattern with α-actinin (Fig. **11a-i** and **11b-i**). Furthermore, M-lines are also in the middle of A-bands. Thus, I analyzed the localization of Myom2-RFP relative to cTnT which appeared as two closely bands in the A-bands of sarcomeres (Fig. **11a-ii** and **11b-ii**), to investigate more detail. Indeed, double staining with cTnT and anti-RFP showed Myom2-RFP was flanked with cTnT (Fig. **11a-ii** and **11b-ii**). These results confirmed that Myom2-RFP was correctly localized to the M-lines of the sarcomeres.

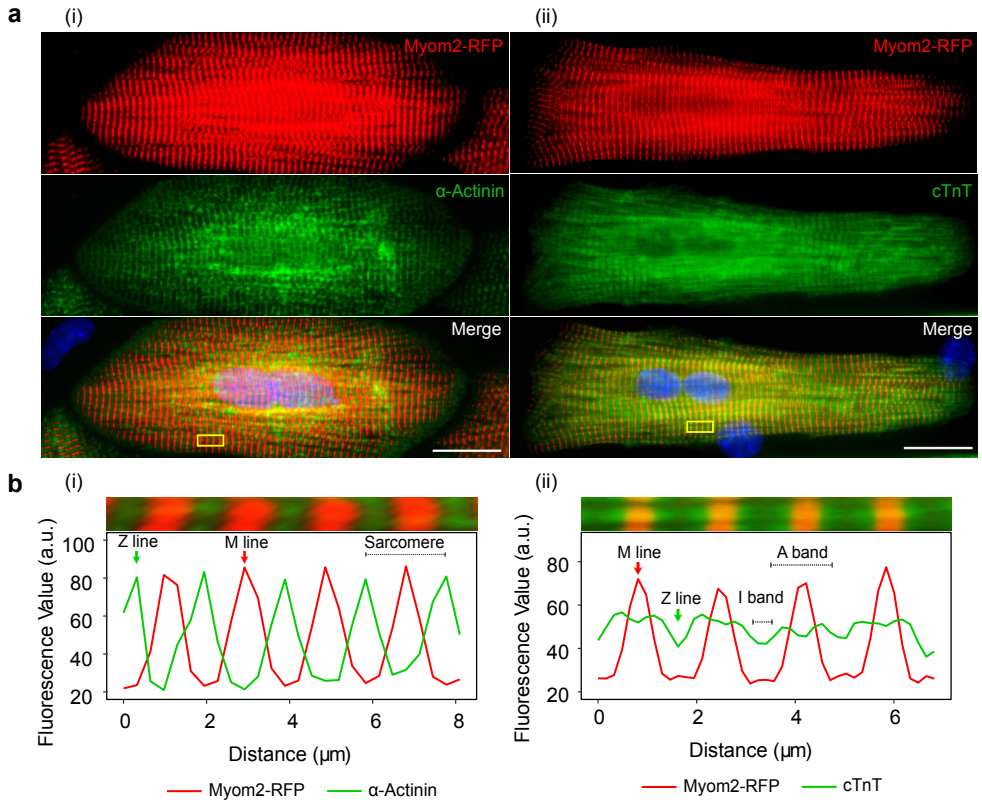

Figure 11. Localization of Myom2-RFP in the PSC-CMs.

(**a**) Immunostaining of Myom2-RFP (red) relative to α-actinin (i) and cTnT (ii) in PSC-CMs. Yellow box regions in each panel are elongated and shown in (**b**). Line scans through the middle of the selected region are presented below, α-actinin (i) and cTnT (ii). Red and green arrows indicate the positions of M- and Z-lines, respectively. Scale bar = 20 μm.

4.2.3) Prolonged culture increases Myom2-RFP expression and RFP intensity

As mentioned in result **4.2.1**, Myom2 expression was upregulated during the myocardial growth of developing mice from E11 to P56 (Fig. **9a**). Thus, I examined Myom2-RFP profile of PSC-CMs generated form the reporter line, to confirm whether knocked-in Myom2 could express similar to that of mouse hearts. To this end, I plated PSC-CMs at day 10 of differentiation on 0.1% gelatin, and then cultured for 18 more days (Fig. **12a**). PSC-CMs in different time points of extended culture (day10, 21, and 28) were quantitatively analyzed both percent of Myom2-RFP$^+$ cells and RFP intensity by fluorescence-activated cell sorting (FACS). Representative images of flow cytometry for Myom2-RFP$^+$ cells are presented in Fig. **12b**. The result showed that Myom2-RFP$^+$ cells could not detect immediately after 10 day of cardiac differentiation (0.78%), whereas a prolonged culture which known to enhance CM maturation[33], increased percent of Myom2-RFP$^+$ cells and RFP intensity from day 21 to day 28 (Fig. **12c**).

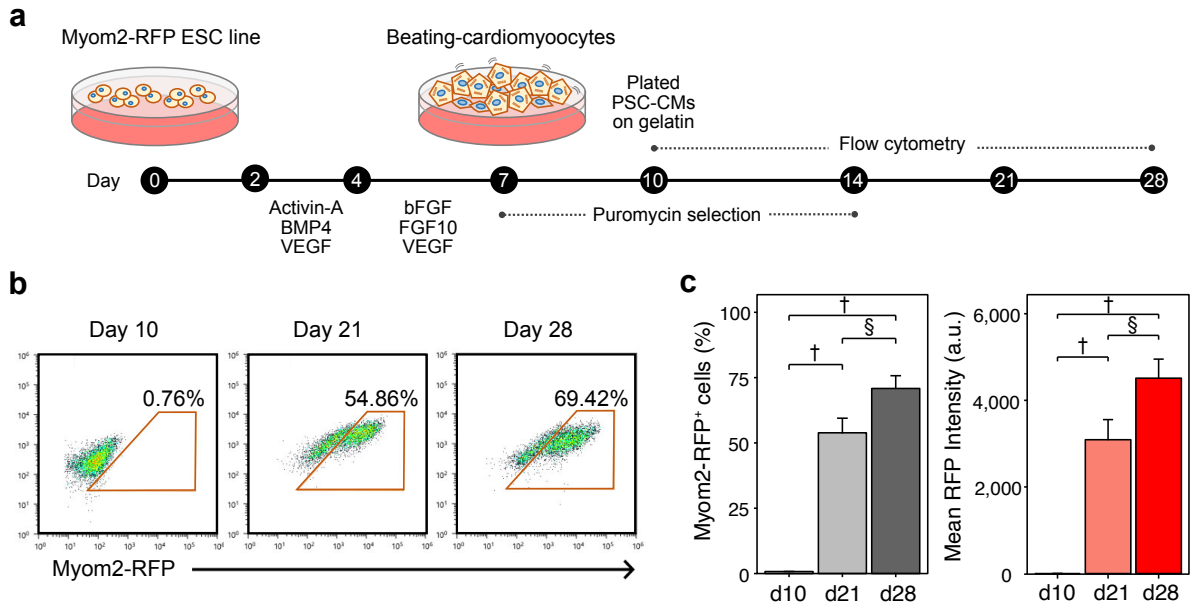

Figure 12. Expression profile of Myom2-RFP.

(**a**) Schematic representation of cardiac differentiation from Myom2-RFP reporter line and extended culture up to day 28. (**b**) Representative images of flow cytometry for Myom2-RFP$^+$ cells. (**c**) Numbers of Myom2-RFP$^+$ cells were increased after the prolonged culture of PSC-CMs. Data are presented as means ± SD (n = 4). One-way ANOVA with posthoc Tukey HSD test; § $P < 0.01$, † $P < 0.0001$. Fluorescence intensity is presented as an arbitrary unit (a.u.).

4.2.4) RFP$^+$ cells display morphologically more mature than RFP$^-$ cells

In a neonatal heart, *Myom2* expression was abundant approximately 500 TPMs which would allow us to observed fluorescence signal. Therefore, I hypothesized that RFP$^+$ cells would mature than RFP$^-$ cells. To test this hypothesis, I compared the morphological difference between RFP$^+$ and RFP$^-$ cells by immunostaining for α-actinin, a sarcomere protein (Fig. **13a**). The result showed that RFP$^+$ cells had longer sarcomere length, increased cell size and perimeter, and showed higher aspect ratio (cell length and width ratio), especially at day 28 (Fig. **13b**). Moreover, RFP$^+$ cells also had higher percent of binuclear cells compared to RFP$^-$ cells (Fig. **13c**). These results indicated that RFP$^+$ cells possessed morphologically mature than RFP$^-$ cells.

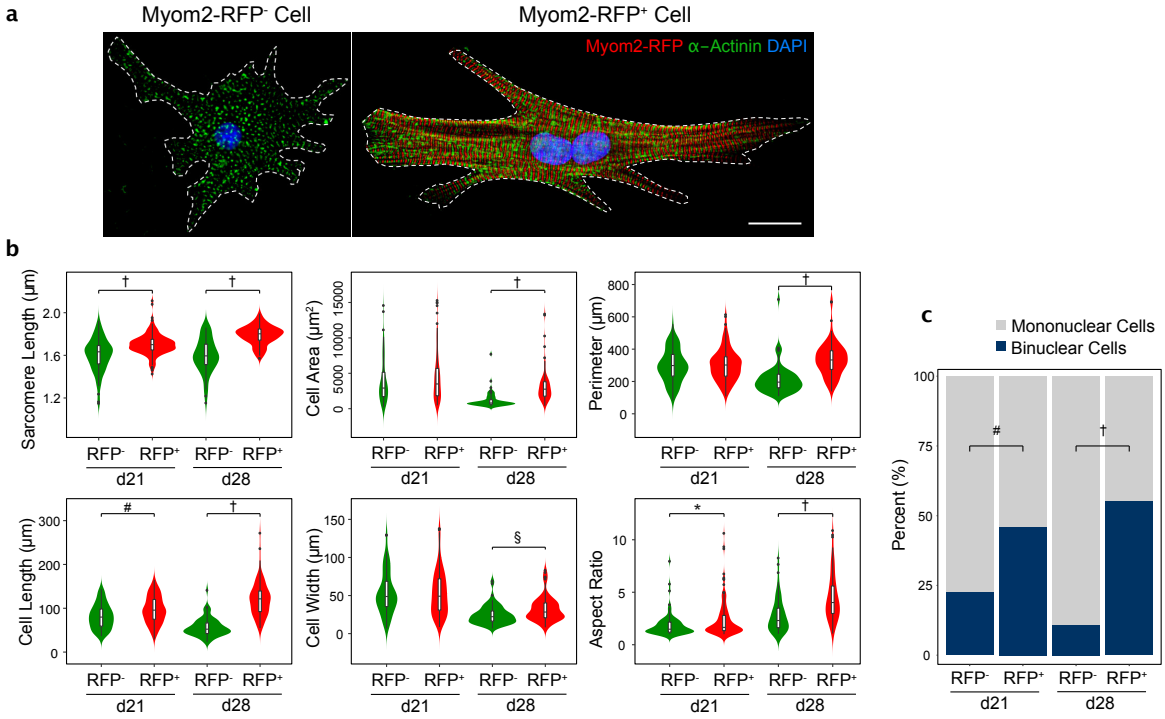

Figure 13. Morphological difference between RFP$^-$ and RFP$^+$ cells.

(**a**) Representative images of RFP$^-$ and RFP$^+$ cells at day 28 of cell culture. Myom2-RFP (red); α-actinin (green); Nuclei (blue). Scale bar = 20 μm. (**b**) Comparisons of structure and morphology between RFP$^-$ and RFP$^+$ cells (n > 65). Several parameters were examined including sarcomere length, cell area, perimeter length, cell length, cell width, and aspect ratio. For violin plots, medians are indicated as black lines in the middle of white boxes; interquartile ranges are showed with the white box in the center of violin plot; the black lines stretched from the boxes indicate first quartile -1.5 interquartile and third quartile +1.5 interquartile, respectively; polygons represent

density estimates of data and extend to extreme values. Student's *t*-test was used to calculate statistical difference; $^{*}P < 0.05$, $^{\S}P < 0.01$, $^{\#}P < 0.001$, $^{\dagger}P < 0.0001$. (**c**) Percent of binuclear cells in RFP^- and RFP^+ cells ($n > 65$). Chi-square Test; $^{\#}P < 0.001$, $^{\dagger}P < 0.0001$. These images are modified from data submitted to *Sci Rep*.

4.2.5) RFP^+ cells show physiologically more mature than RFP^- cells

In addition, RFP^+ cells were expected to improve their physiology towards adult-like CMs such as calcium handling property and sarcomere shortening. To examine intracellular calcium transients in RFP^- and RFP^+ cells, time-lapse images were recorded at a stimulation frequency of 1 Hz (Fig. **14a**). The corresponding amplitudes ($\Delta F/F_0$) of calcium transients were shown in Fig. **14b**. As expected, RFP^+ cells had higher peak calcium amplitude and time to decay faster than RFP^- cells, while time to peak of the calcium transients was no significant difference (Fig. **14c**).

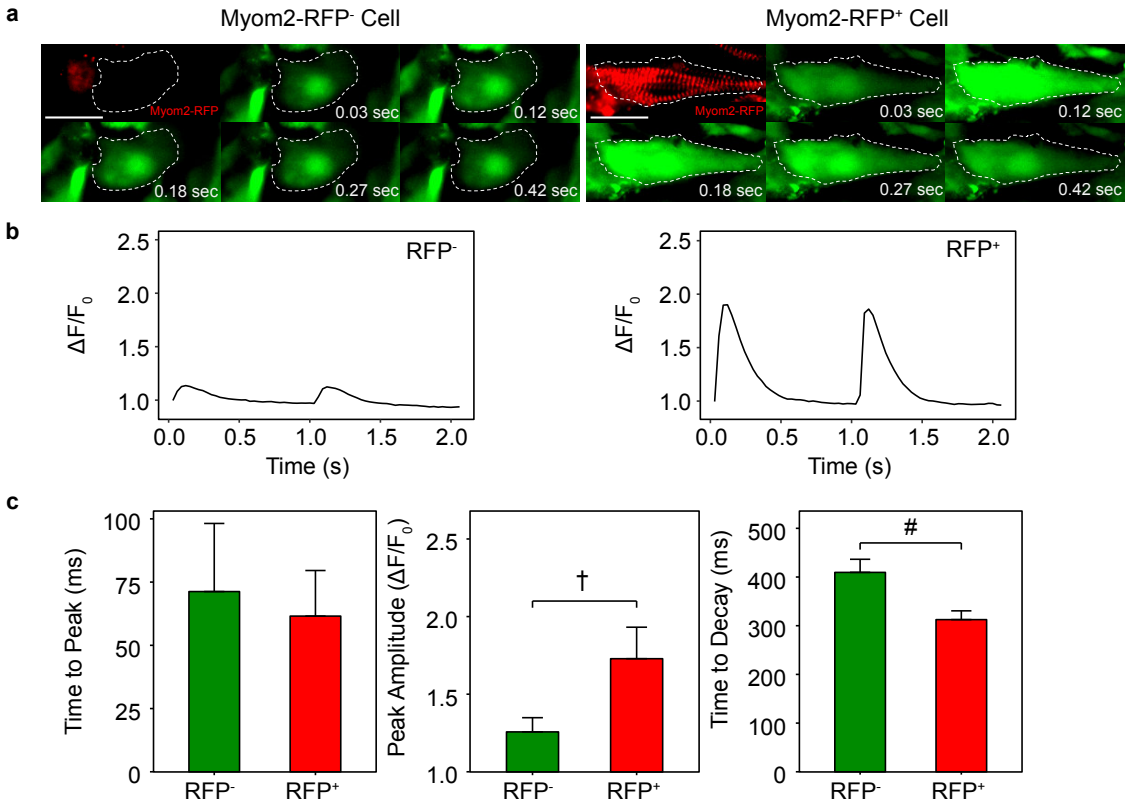

Figure 14. Comparison of calcium handling between RFP^+ and RFP^- cells.
(**a**) Representative recording of calcium transients in RFP^+ and RFP^- cells, scale bar = 20 μm. (**b**) The corresponding amplitudes ($\Delta F/F_0$) of calcium transients by electrical field stimulation at 1 Hz, at day 28. $\Delta F/F_0$ value was calculated by fluorescence (F) minus with background followed by normalizing to baseline fluorescence (F_0). (**c**)

Quantifications of time to peak, calcium transient amplitude, and time to decay. Data are shown as means ± SD (n > 30). Student's t-test; $^{\#}$ P < 0.001, † P < 0.0001. These images are modified from data submitted to *Sci Rep*.

With the advantage of using knocked-in fluorescence into sarcomere protein, I could obtain sarcomere shortening, which is hardly observed in PSC-CMs. To determine sarcomere shortening, time-lapse images for detecting RFP signal were recorded during CM contraction (Fig. **15a**). RFP^{+} cells exhibited contraction steadily, and sarcomere shortening was approximately 6.8% (from about 2.03 ± 0.19 μm down to 1.89 ± 0.20 μm) (Fig. **15b-c**). Altogether, RFP^{+} cells were more mature than RFP^{-} cells in terms of morphology, structure, and function. Thus, the Myom2-RFP reporter line can be used as a CM maturation reporter.

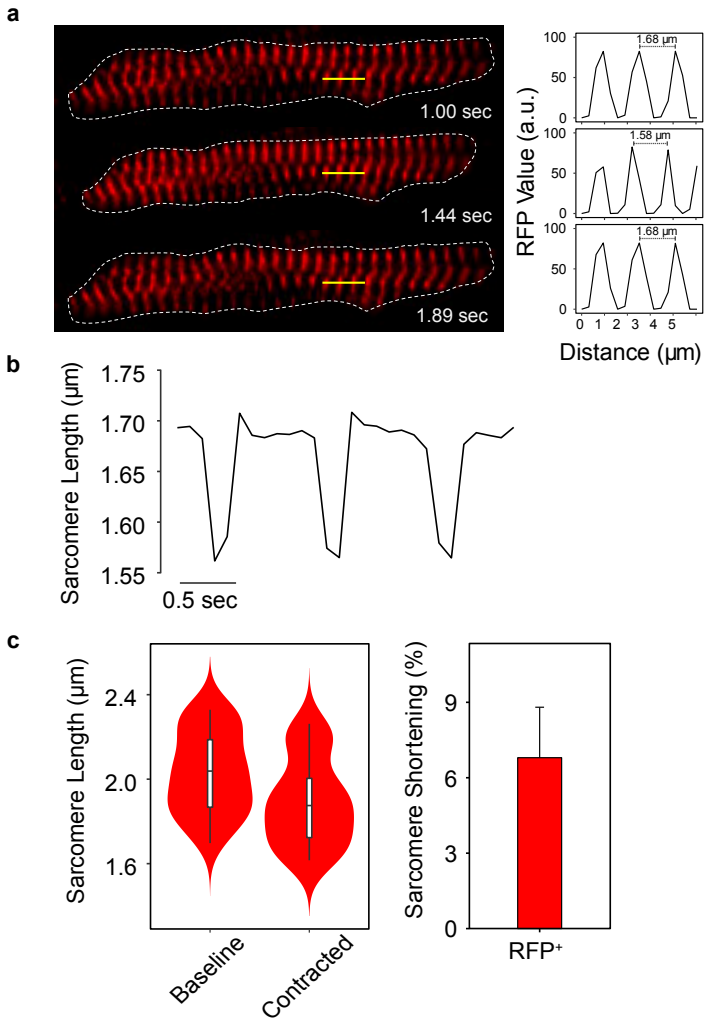

Figure 15. Sarcomere shortening assay in RFP^{+} cells.
(**a**) Representative images of cell shortening with typical line scan of sarcomere length obtained from yellow lines in the images on the left panel. (**b**) The corresponding sarcomere shortening profile of RFP^{+} cells. (**c**) sarcomere length in relaxed and contracted forms and percent of cell shortening of RFP^{+} cells (n = 38). Violin plots are described in Fig. **13**. These images are modified from data submitted to *Sci Rep*.

4.3) Development of a quantitative method for CM maturation

Previously, our group has developed a microarray-based quantitative assay for CM maturation[1]. I recently updated the method with Quant-seq, 3' mRNA-sequencing, that requires less read depth and allows more multiplexing samples per a single run with affordable cost than standard RNA sequencing (Fig. **16a**). Here, I collected hearts both atria and ventricles from E11 to 10 months postnatal of developing mouse. Then, transcriptomes were obtained by RNA sequencing. Principal component analysis (PCA) revealed that each stage of CMs was separated by the differential gene expressions along the PC1-axis, whereas PC2-axis obviously discriminated atria and ventricle from each other (Fig **16b**). With the updated method, I have set a weight for each gene in PC1-axis of ventricles to the calculate maturation score. The maturation score is sum of the expression levels of each gene (transcript per million reads, TPM) multiplied by the weight (Method **3.5**). The score increases linearly from embryo to adult heart, indicating the success of calculation of maturation score (Fig. **16c**).

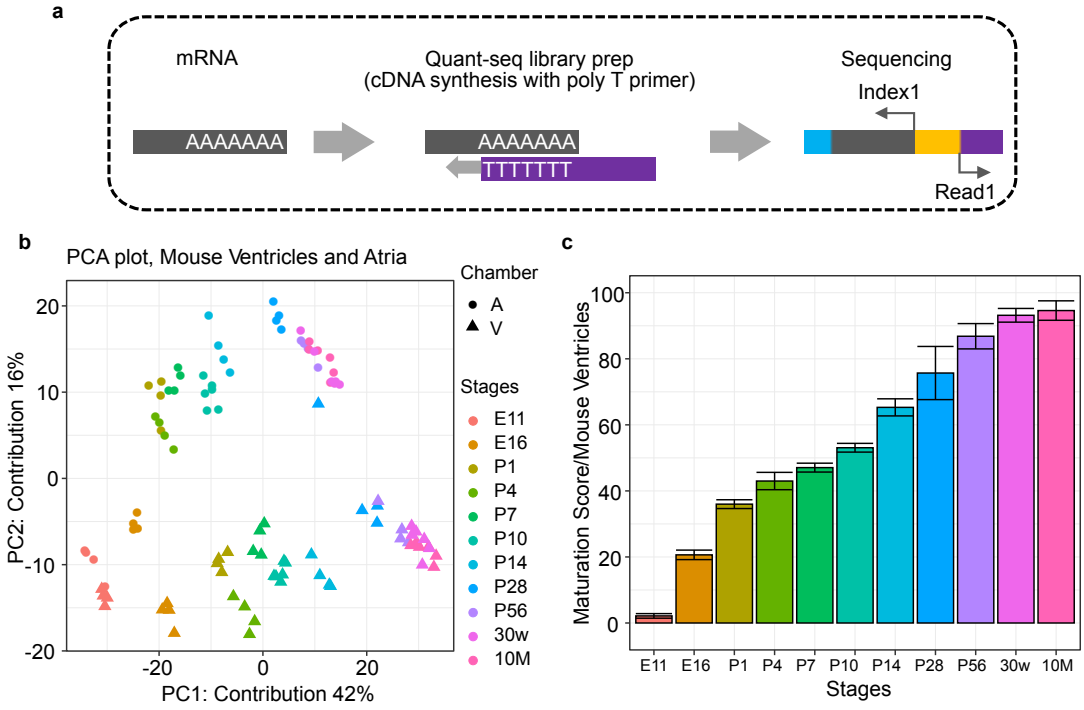

Figure 16. Development of a quantitative method for CM maturation.
(**a**) Schematic representation of the experimental workflow for Quant-seq. (**b**) PCA plot was performed on transcriptome data derived from mouse hearts at different ages ranging from E11 to 10 months postnatal. (**c**) Maturation score in mouse hearts.

4.3.1) RFP$^+$ cells are more mature than RFP$^-$ cells

To compare the maturity of RFP$^-$ and RFP$^+$ cells, I next sorted the cells after prolonged culture for 17, 24, and 38 days, and assessed the maturation scores in accordance with the protocol mentioned in Method **3.5**. Furthermore, I also assessed the maturity of PSC-CMs at day 10, to use as a baseline for maturation (Fig. **17**, right panel). The result showed that the maturation scores of both RFP$^-$ and RFP$^+$ cells were soon increased right after cardiac differentiation for 10 days. Although, the maturation scores of RFP$^-$ cells increased, but it still lower than those of RFP$^+$ cells in any time points, suggesting RFP$^+$ cells were more mature than RFP$^-$ cells, which consistence with morphological and physiological analysis. Notably, RFP$^+$ cells at day 38 showed the highest maturation score which was a similar degree of CMs in between P7 to P10 (Fig. **17**, left panel). This result demonstrated that the PSC-CMs remained immature even though prolonged culture for a course of a month. Therefore, applying additional enhancers for CM maturation are required to obtain adult-like mature CMs.

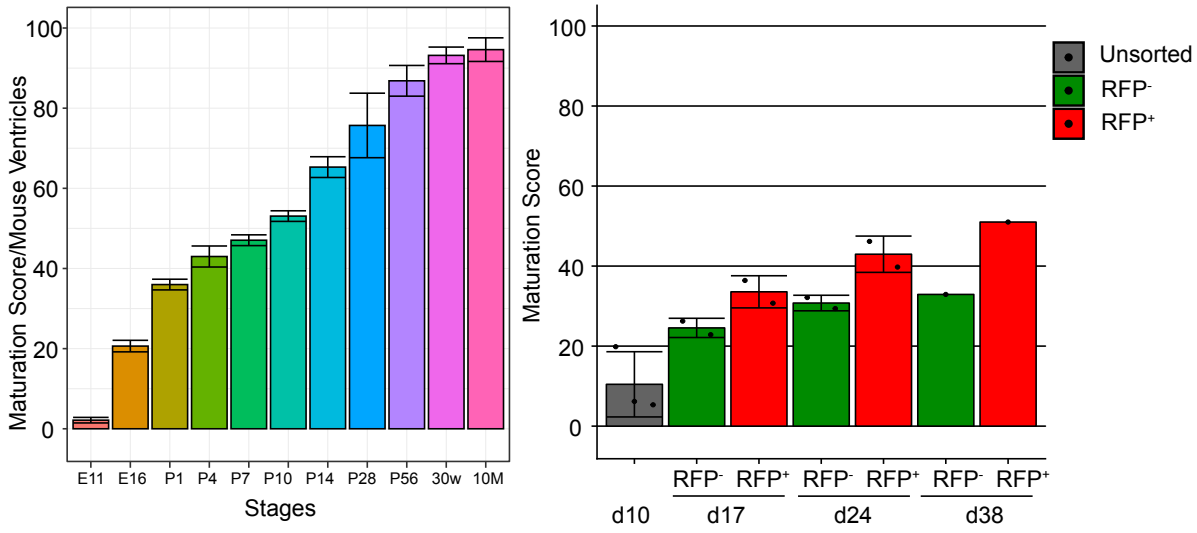

Figure 17. Maturation degree of RFP$^-$ and RFP$^+$ cells.

The maturation scores of RFP$^-$ and RFP$^+$ cells at different time points including day 17, 24 and 38 (right panel), and PSC-CMs at day 10, were compared to those of mouse heart counterparts (left panel). Black dots represent maturation scores of each sample.

4.3.2) RFP$^+$ cells have transcriptionally more mature than RFP$^-$ cells

In addition to morphology and physiology, I also confirmed if RFP$^+$ cells are more mature than RFP$^-$ cells in terms of gene transcription. With analyzing the transcriptome data from result **4.3.1**, I found that CM maturation-related genes were highly upregulated in RFP$^+$ cells such as sarcomere genes (*Myh7*, *Myl2*, *Myl3*, *Myoz2*, and *Mypn*), calcium-handling gene (*Casq2*), and ion transporter at sarcolemma (*Kcna4*) (Fig. **18a**). Furthermore, gene ontology (GO) analysis revealed that GO terms involved in structural construction and muscle development are enriched in RFP$^+$ cells, while GO terms of ECM organization were highly enriched in RFP$^-$ cells (Fig. **18b**).

In early heart development, glycolysis is a primary source of energy production for proliferating CMs. As CMs reach to terminal stage of differentiation, mitochondrial oxidative capacity increase, and fatty acid β-oxidation become a major energy source for the heart. The switch from glycolysis to mitochondrial metabolism during heart development results from the alteration of gene transcription to control each metabolic pathway[18]. To explore the transcriptional changes, I examined overall gene expression levels in selected GO terms of biological processes (Fig. **18c**). Surprisingly, genes related to glucose metabolism and cell cycle were downregulated after 10 days of cardiac differentiation, but these sets of genes were more gradually downregulated in RFP$^+$ cells after prolonged culture for 24 and 38 days, respectively (Fig. **18c-i and v**). Consistent with the metabolic switch during cardiac development, genes in lipid metabolic process, fatty acid β-oxidation, and mitochondrion were upregulated in RFP$^+$ cells when compared to RFP$^-$ cells, implying that a metabolic switch was occurring in RFP$^+$ cells (Fig. **18c-ii to iv**). Moreover, Genes in myofibril assembly, cardiac muscle tissue development, and T-tubule organization were highly upregulated in RFP$^+$ cells (Fig. **18c, vi to viii**). These results supported that RFP$^+$ cells were transcriptionally more mature than RFP$^-$ cells.

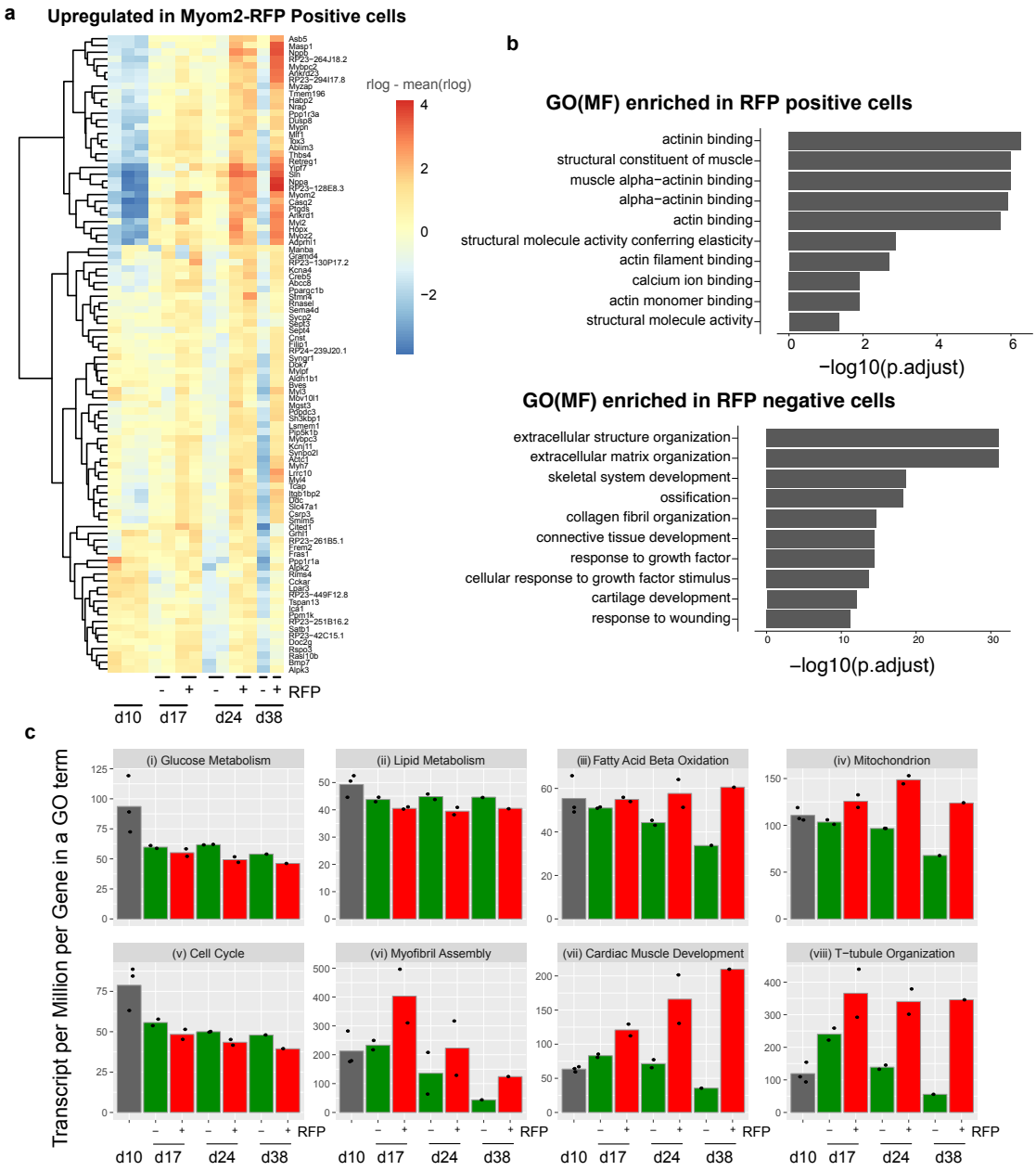

Figure 18. RNA-seq analysis of RFP$^-$ and RFP$^-$ cells.

(**a**) Gene expression profile of RFP$^+$ PSC-CMs at different time points of a prolonged culture compared to RFP$^-$ cells. Rlog values are coded on the red-to-blue scale (higher expression, red; lower expression, blue). (**b**) GO terms for molecular function identify for differentially enriched genes in RFP$^+$ and RFP$^-$ cells. The x-axis represents the logarithms of the adjusted *p*-value. (**c**) Averaged gene expression of 8 selected GO terms for biological processes including, (i) glucose metabolism, (ii) lipid metabolism, (iii) fatty acid β-oxidation, (iv) mitochondrion, (v) cell cycle, (vi) myofibril assembly, (vii) cardiac muscle development, and (viii) T-tubule organization. These images are modified from data submitted to *Sci Rep*.

4.4) Evaluation of the effects of ECMs on CM maturation

4.4.1) Identifications of candidate ECMs for CM maturation

Since developing CMs in the heart are exposed to several ECMs, it seems likely that ECMs will lead to better maturation of PSC-CMs. Therefore, I examined the effects of ECMs on PSC-CMs maturation. ECMs not only contain important signaling molecules, but also provide structural support for myocardium. There were plenty of ECMs expressed as dynamic changes during heart development. To identify candidate ECMs that would enhance CM maturation, I collected RNA from wild-type mouse ventricles ranging from E11 to P56, and performed RNA-sequencing. The hierarchical clustering showed the groups of gene expression patterns among early embryonic, neonatal, and adult ventricles (Fig. **19**).

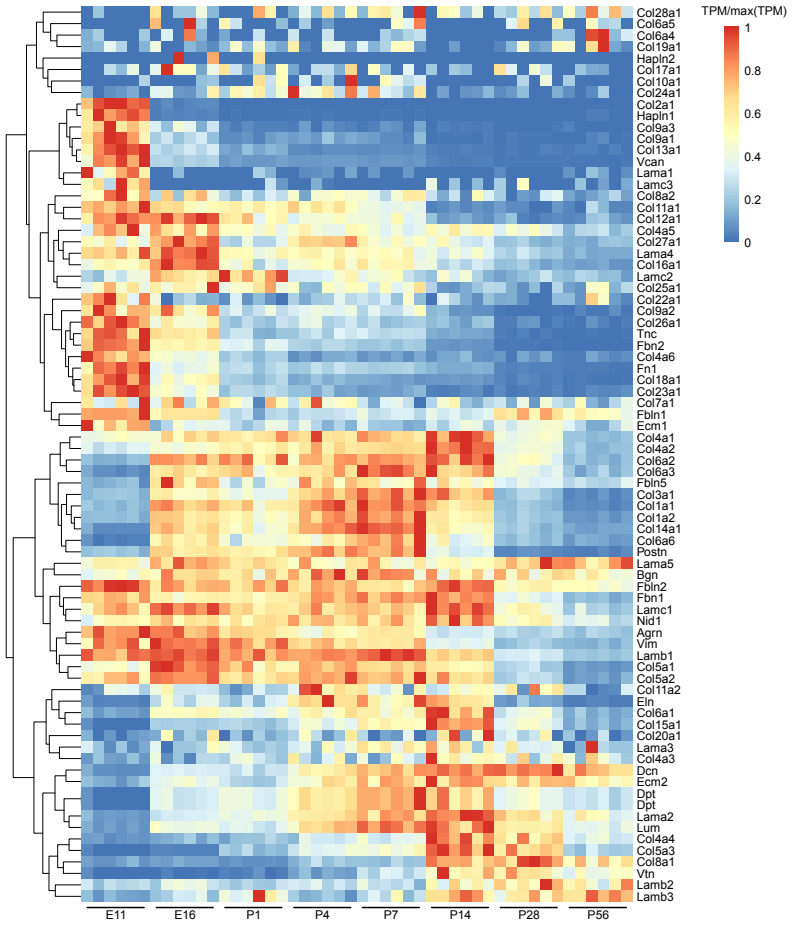

Figure 19. Expression profiles of ECMs during heart development.

A heatmap represents the expressions of various ECMs during heart development (E11 to P56). Colors are coded on the red-to-blue scale of normalized transcripts per million reads (TPM) divided by the highest expression level (TPM/max: high expression, red; low expression, blue).

Among of the ECM expressions, collagen type II (*Col2a1*) and type IV (*Col4a6*), and fibronectin (*Fn1*) were highly expressed in embryonic hearts, whereas collagen type I (*Col1a1* and *Col1a2*) and III (*Col3a1*) were abundantly upregulated in neonatal hearts (Fig. **20**). Moreover, various laminin subunits (such as α2, α5, and β2 chains), as well as one of collagen type IV members (*Col4a4*) were expressed later in adult hearts (Fig. **20**). Altogether, I expected that laminin, collagen, and fibronectin, would affect PSC-CMs maturation *in vitro*.

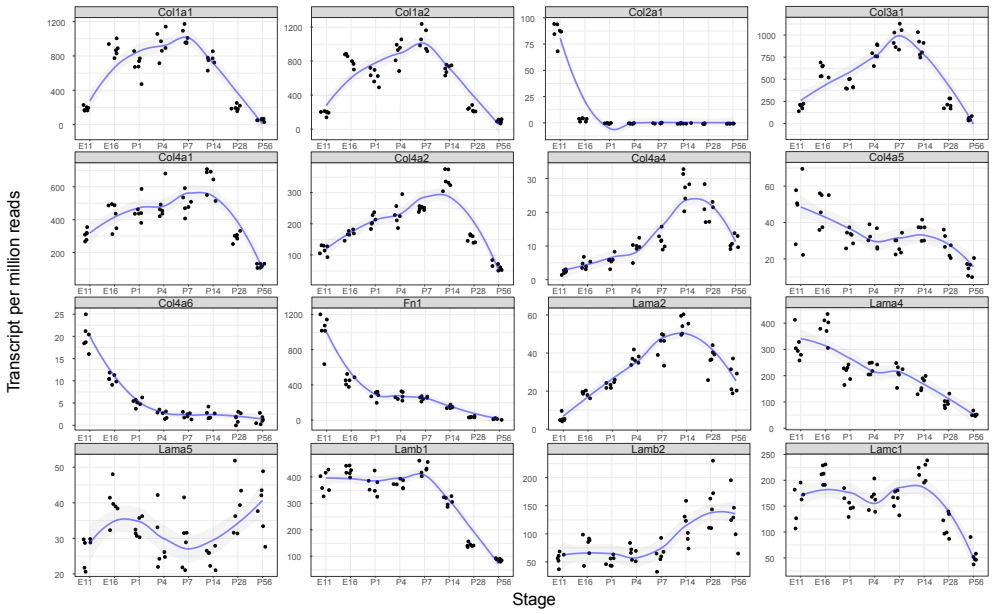

Figure 20. ECM expression profiles during heart development.
Selected ECMs including laminin, collagen, and fibronectin, showed dynamic changes in their expressions from E11 to P56 of mouse hearts. These images are modified from data submitted to *Sci Rep*.

4.4.2) ECMs enhance CM maturation rather than initiating the maturation

To evaluate the effects of ECMs on CM maturation, I plated PSC-CMs generated for Myom2-RFP reporter line, on different concentrations of ECMs ranging from 0.125 to 1 μg/cm^2 at day 10 of cardiac differentiation. The ECMs were tested in this study including various isoforms of laminin E8 fragments (LN-111, 121, 211, 221, 311, 321, 332, 411, 421, 511, and 521), several members of collagen (type I, III, and IV), and fibronectin. To quantitatively determine the proportion of RFP$^+$ cells and RFP intensity, flow cytometry was performed at day 17, 24, and 38, in accordance with the protocol mentioned before in Method **3.4** (Fig. **21a**). Although the fractions of RFP$^+$ cells were not changed when compared to gelatin (Fig. **21b**), all of the tested ECMs

dose-dependently increased RFP intensity of PSC-CMs, indicating the impacts of ECMs on CM maturation (Fig. **21c**). The results of 1 μg/cm^2 of ECMs at day 38 of differentiation were summarized in Fig. **21d**. PSC-CMs plated on laminin-511/521 had the highest RFP intensity than other ECMs. This result implied that ECMs likely promoted CM maturation rather than initiating the maturation.

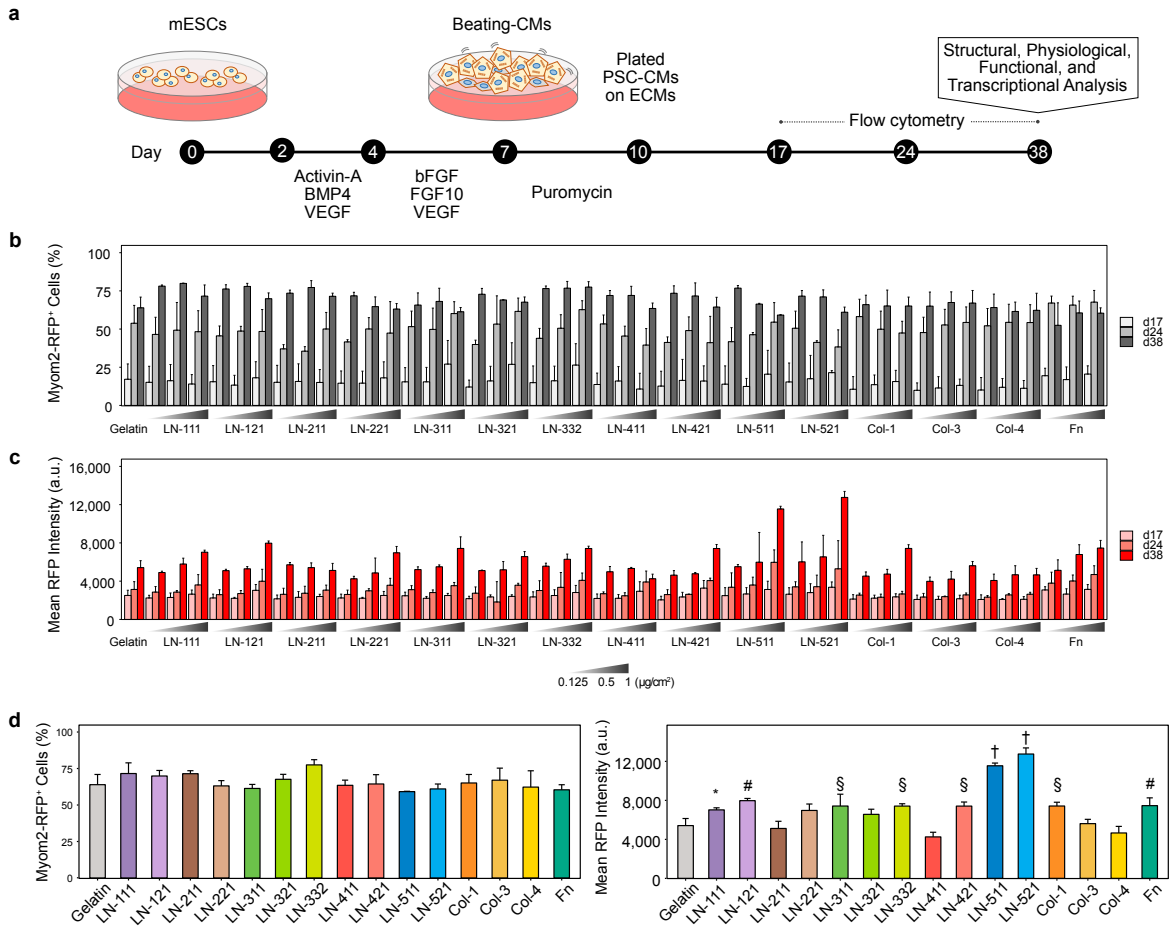

Figure 21. Effects of ECMs on CM maturation.

(**a**) Schematic representation of experimental design for culturing PSC-CMs on ECMs after cardiac differentiation. (**b**) Percent of RFP$^+$ cells and (**c**) RFP intensity at day 17, 24, and 38. ECM concentrations are shown at 0.125, 0.5, and 1.0 μg/cm^2. Data are presented as means ± SD (n = 3). Fluorescence intensity is presented as arbitrary units (a.u.). (**d**) Quantification of RFP$^+$ cells (left panel) and RFP intensity (right panel) of 1 μg/cm^2 of ECMs at day 38 of cell culture. Data are presented as means ± SD (n = 3). Dunnett's test was used to compare between ECMs versus control (gelatin); $^*P < 0.05$, $^§ P < 0.01$, $^\# P < 0.001$, $^† P < 0.0001$. These images are modified from data submitted to *Sci Rep*.

4.4.3) ECMs promote morphological and structural maturation of PSC-CMs, especially laminin-511/521

To determine the morphology and structure of PSC-CMs plated on ECMs, immunostaining for α-actinin and TagRFP was conducted (Fig. **22a**). Interestingly, only laminin-511/521 showed significant increases in the sarcomere length of PSC-CMs. Moreover, PSC-CMs on gelatin were small in shape, whereas the cells on laminin-511/521 significantly increased cell area, cell length, and cell width (Fig. **22b**). Besides, PSC-CMs plated on laminin-511/521 also showed the highest proportion of binuclear cells (Fig. **22c**). These results implicated that laminin-511/521 enhanced CM maturation.

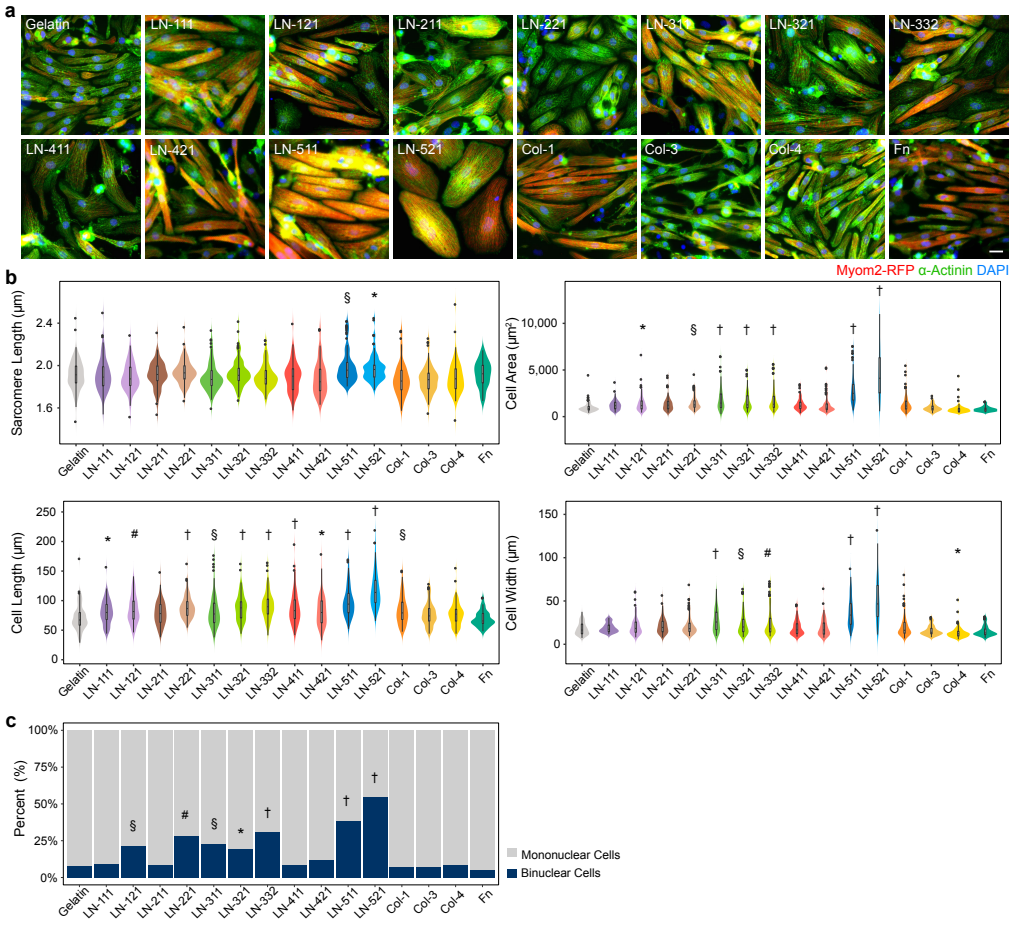

Figure 22. Morphological and structural differences in the treated PSC-CMs. (**a**) Representative images for PSC-CMs plated on different ECMs at day 38. The cells were labeled of α-actinin (green), TagRFP (red), and DAPI for nuclei (blue). Scale bar = 20 μm. (**b**) Statistics of structural and morphological features. Sarcomere length, cell area, cell length, and cell width were examined. Violin plots are described in Fig. **13** (n > 100 from three different cardiac differentiation runs). Dunnett's test was used to

compare between ECMs versus control (gelatin); $^{*}P < 0.05$, $^{\S}P < 0.01$, $^{\#}P < 0.001$, $^{\dagger}P < 0.0001$. (**c**) Percent of binuclear cells of PSC-CMs cultured on different ECMs ($n > 100$). Chi-square Test; $^{*}P < 0.05$, $^{\S}P < 0.01$, $^{\#}P < 0.001$, $^{\dagger}P < 0.0001$. These images are modified from data submitted to *Sci Rep*.

4.4.4) Laminin-511/521 promote localization of Cx43 to lateral cell-axis

The intercalated disk at the longitudinal cell-edges of CMs provides as a macromolecular infrastructure that integrates mechanical and electrical coupling within the heart. Previous study found that gap junction protein, Cx43, localized to intercalated disk when CM mature[11]. In PSC-CMs, the membrane localization of Cx43 required dense culture conditions to allow the formation of cell-cell junction sites[94]. Thus, I hypothesized that if laminin-511/521 enhance CM maturation, they would affect the localization of Cx43. To prove this hypothesis, I performed immunostaining at day 38 of cell culture (Fig. **21a**). I found that RFP^{+} cells were grown as a sparse pattern when plated PSC-CMs on gelatin, and only showed low expression of Cx43 which appeared around perinuclear. Surprisingly, laminin-511/521 promoted the formation of RFP^{+} cell connections and the monolayer of rod-shape cells, resulting in localization of Cx43 to lateral cell-axis which better than gelatin (Fig. **23**).

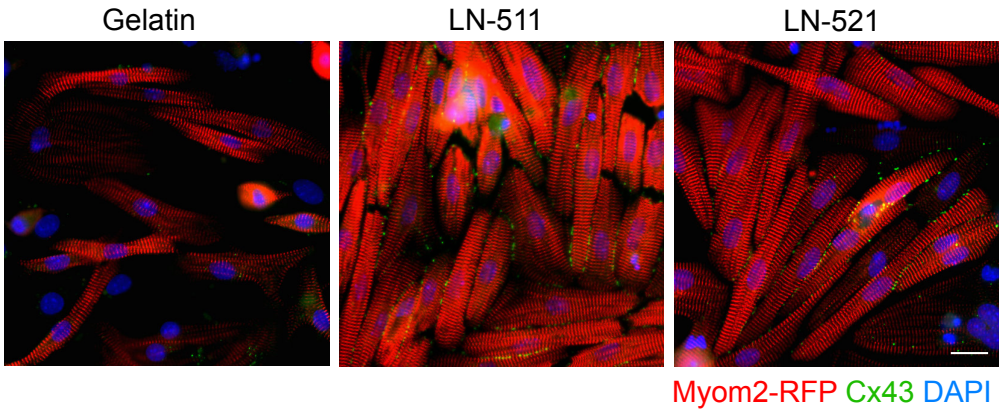

Figure 23. Localization of Cx43 in PSC-CMs plated on laminin-511/521. Representative PSC-CMs plated on laminin-511/521 stained for TagRFP (red), Cx43 (green), and DAPI for nuclei (blue). Laminin-511/521 induced localization of Cx43 to lateral cell-axis compared to gelatin (control). Scale bar = 20 μm. These images are modified from data submitted to *Sci Rep*.

4.4.5) Laminin-511/521 promote functional maturation of PSC-CMs

The Seahorse XF96 extracellular flux analyzer was used to examine mitochondrial function as previously described in Method **3.8**. In this assay, oxygen consumption rate (OCR) was measured in real-time in basal respiration and in response to ATP synthase inhibitor (oligomycin), mitochondrial uncoupler (FCCP), as well as the respiratory chain blockers (rotenone/antimycin A), respectively (Fig. **24a**). Although ATP-linked respiration was no significant difference, base-line mitochondrial respiration and maximum respiration capacity were elevated in the laminin-511/521 (Fig. **24b-i, ii, and iv**). Proton leak was also exhibited substantially higher in laminin-511 condition (Fig. **24b-iii**). These results supported that laminin-511/521 enhanced functional maturation of PSC-CMs.

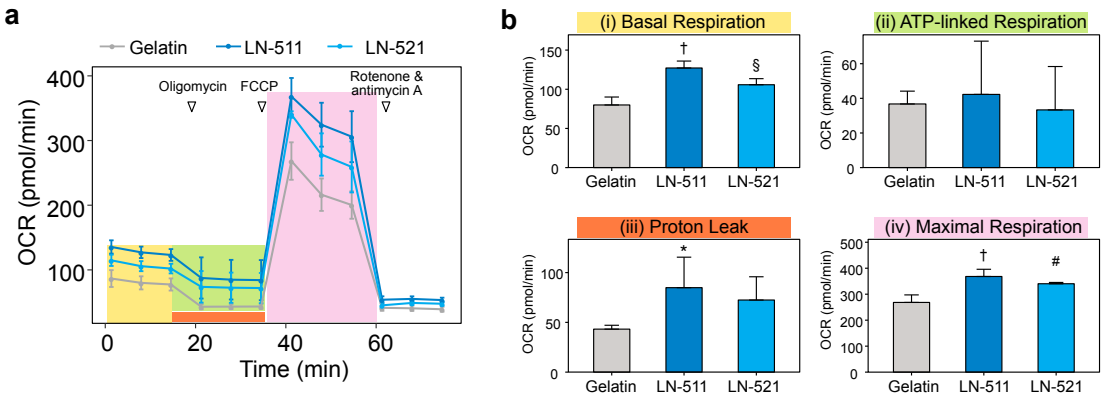

Figure 24. The effects of laminin-511/521 on mitochondrial function.

(**a**) Representative traces for control (gelatin) and laminin-511/521 responding to oligomycin (ATP synthase inhibitor), FCCP (the respiratory uncoupler), and rotenone/antimycin A (the respiratory chain blockers). Data are shown as means ± SD (n = 3 from three different cardiac differentiation runs). (**b**) Statistical analysis of mitochondrial respiration, ATP-linked respiration, the difference in proton leak, and maximum mitochondrial respiration capacity. Dunnett's test; $^{*}P < 0.05$, $^{\S}P < 0.01$, $^{\#}P < 0.001$, $^{\dagger}P < 0.0001$. These images are modified from data submitted to *Sci Rep*.

4.4.6) Laminin-511/521 improve physiological changes of PSC-CMs

Furthermore, I also examined physiological changes of PSC-CMs which were cultured on laminin-511/521 compared to gelatin. Similar to the characterizations of RFP^{-} and RFP^{+} cells, the physiological changes were tested including calcium

transients and sarcomere shortening. To investigate potential effects of laminin-511/521 on calcium kinetics, I loaded Calbryte 520-AM to PSC-CMs and stimulated the cells under 1 Hz electrical pulse. Representative traces are shown in Fig. **25a**. The result demonstrated that laminin-511 led to a significant increase in peak amplitude of calcium transients, whereas laminin-521 showed faster time to peak and time to decay compared to gelatin (Fig. **25b**). For sarcomere shortening, the time-lapse images for RFP signal were recorded as the same stimulated condition with calcium transients. Representative traces for sarcomere shortening are shown in Fig. **25c**. The result showed that laminin-511/521 increased percent of sarcomere shortening compared to gelatin (Fig. **25d**). These results indicated that laminin-511/521 improved the physiological properties of PSC-CMs.

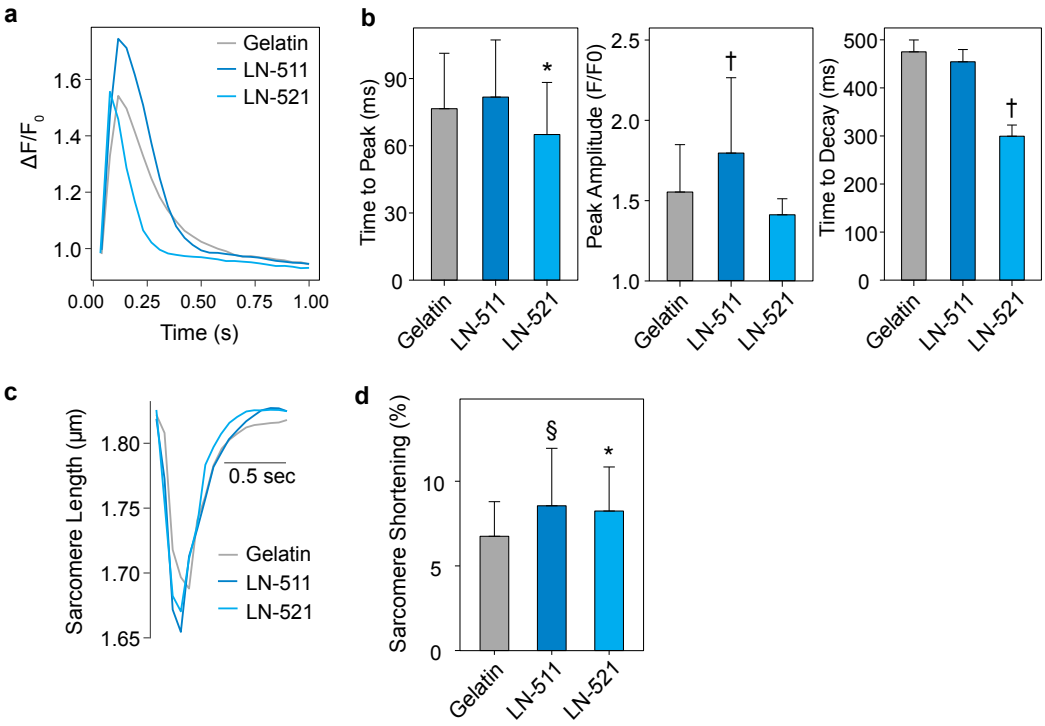

Figure 25. Physiological changes of PSC-CMs plated on laminin-511/521.
(**a**) Intracellular calcium transients of PSC-CMs plated on gelatin (gray), laminin-511 (dark blue), and laminin-521 (light blue), under electric pacing at 1 Hz. (**b**) Statistical analysis of time to peak, peak amplitude, and time to decay. Dunnett's test; $^{*}P < 0.05$, $^{\dagger}P < 0.0001$. (**c**) Representative recording traces of PSC-CMs cultured on gelatin (gray), laminin-511 (dark blue), and laminin-521 (light blue), under electric pacing at 1 Hz. (**d**) Percent of sarcomere shortening of PSC-CMs plated on different ECMs. Dunnett's test; $^{*}P < 0.05$, $^{\S}P < 0.01$. These images are modified from data submitted to *Sci Rep*.

4.4.7) Laminin-511/521 induce cardiac gene expressions

To determine the maturity of PSC-CMs plated on laminin-511/521, I collected RNA from each condition at day 24 and 38, and performed RNA sequencing. The maturation scores were calculated as mentioned in Method **3.5**. The result showed that prolonged culture of PSC-CMs from day 24 up to day 38, was slightly increased maturation scores, especially gelatin and laminin-511 (Fig. **26**, right panel). Compared to mouse hearts, the PSC-CMs plated on laminin-511 at day 38 had maturation score in between P10 to P14, whereas laminin-521 was in between P7 to P10. Moreover, the maturation score of PSC-CMs plated on laminin-511 at day 38 was slightly increased compared to gelatin.

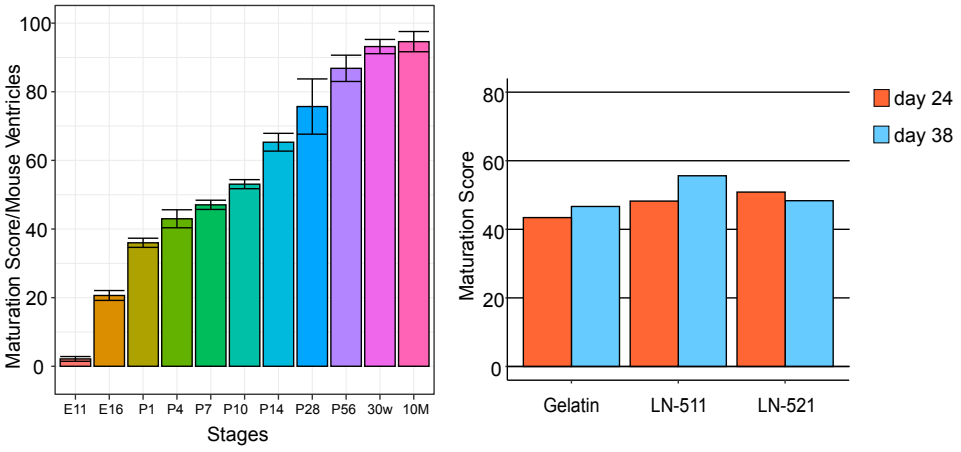

Figure 26. Maturation scores of PSC-CMs plated on laminin-511/521.
After cardiac differentiation for 10 days, PSC-CMs were plated on laminin-511/521 and gelatin (control). Cells were then cultured for more 14 and 28 days. At each time point, RNA was collected, and subjected to RNA-sequencing to determine the maturation scores (right panel).

Next, I analyzed the transcriptome data to examine if laminin-511/521 affect any set of gene expressions specific to biological processes (Fig. **27a**). The result revealed that PSC-CMs cultured on laminin-511/521 had similar level of those processes compared to gelatin (Fig. **27a**). However, when I focused on particular genes related to CM maturation, PSC-CMs cultured on laminin-511/521 resulted in upregulations of cardiac marker (*Tnnt2*), cardiac muscle (*Actc1*), transcriptional regulator (*Ankrd23*), calcium handling (*Casq2*), and sarcomere genes (*Mybpc2*,

Mybpc3, *Myh7*, *Myl2*) (Fig. **27b**). These results indicated that laminin-511/521 induced expressions of gene related to CM maturation.

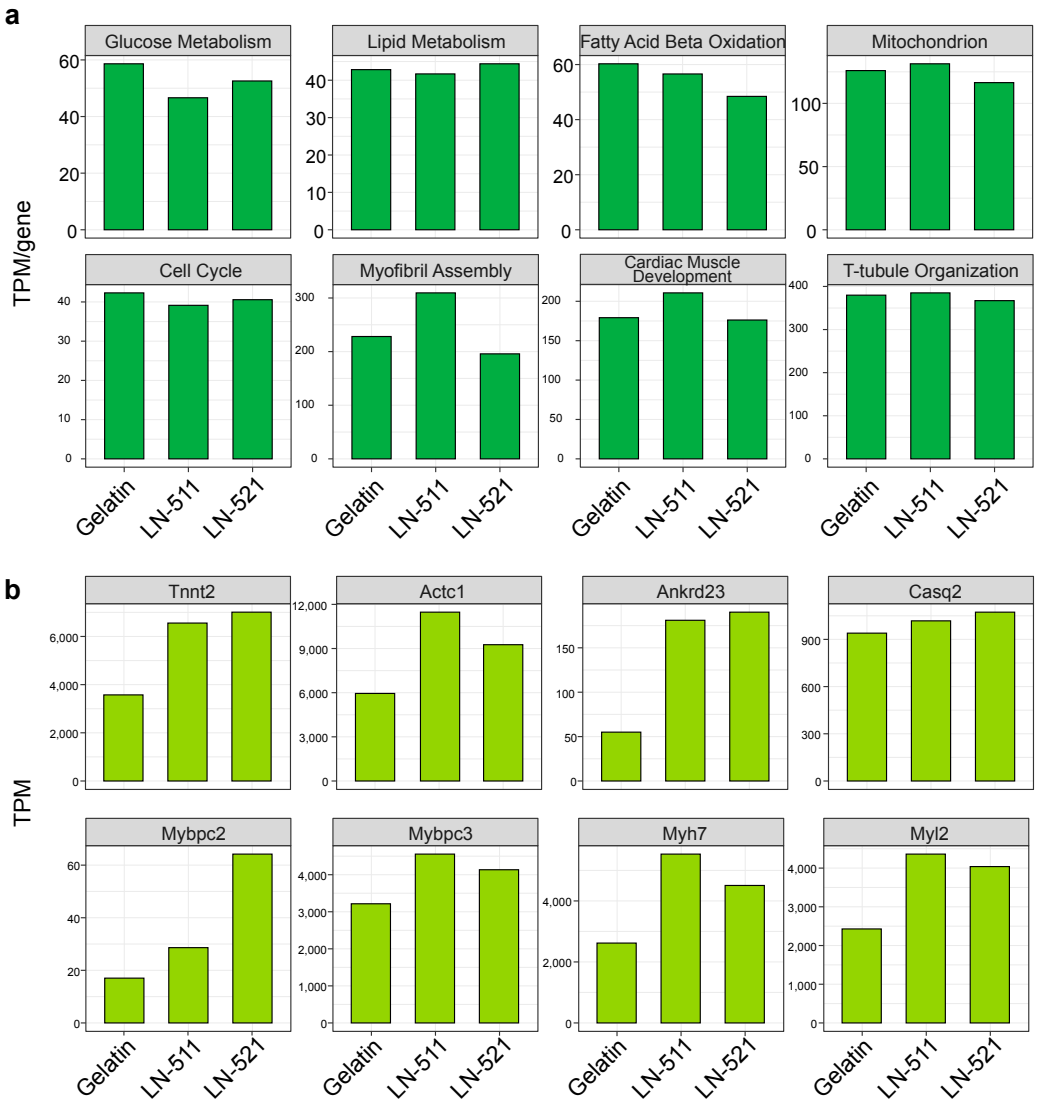

Figure 27. Summaries of biological processes and cardiac gene expressions.
(**a**) Averaged gene expression of 8 selected GO terms for biological processes including, glucose metabolism, lipid metabolism, fatty acid β-oxidation, mitochondrion, cell cycle, myofibril assembly, cardiac muscle development, and T-tubule organization. (**b**) Summary of cardiac gene expressions such as sarcomere genes, transcriptional regulators, gene correlated cardiac functions, and cardiac marker. TPM, transcripts per million reads.

Chapter 5
Summary and Discussion

Heart development is a complex process with temporal and spatial gradients of myriad molecules. Since the critical stages of cardiac specification have been recapitulated through the sequential addition of cytokines, PSCs efficiently give rise to CMs, PSC-CMs. However, as this is the very first phase to be fully functional matured CMs, the PSC-CMs simply display immature phenotypes and limit their use for clinical translations. Previous study has shown that ECMs could enhance CM maturation[48]. However, the maturation degrees of the PSC-CMs with those ECMs remain unknown and no appropriate assessment method to determine the effects of ECMs to CM maturation. Here, I successfully developed qualitative and quantitative methods to assess CM maturation. For qualitative method, I generated a novel Myom2-RFP reporter line, using CRISPR/Cas9 system. After cardiac differentiation, RFP^+ cells were observed and increased throughout the experimental process, which is a corresponding increase in the maturity of PSC-CMs. RFP^+ cells were improved their morphology and physiology towards adult-like mature CMs. Morphologically, RFP^+ cells had long sarcomere length, increased cell area and aspect ratio, and showed higher proportion of binuclear cells compared to gelatin. For physiology, RFP^+ cells had improved calcium handling property by which they had higher peak amplitude and reduced time to decay. In addition to calcium transients, these cells also displayed contraction steadily and sarcomere shortening ~6.8%. For quantitative method, transcriptome data from PSC-CMs were compared to mouse heart counterparts. The results revealed that RFP^+ cells closely resemble relatively mature CMs. These RFP^+ cells co-expressed sarcomere genes (*Myh7*, *Myl2*, *Myl3*, *Myoz2*, and *Mypn*), calcium-handling gene (*Casq2*), and ion transporter at sarcolemma (*Kcna4*). RFP^+ cells also expressed the cardiac muscle gene (*ACTC1*). However, it is well known from previous studies, PSC-CMs are immature compared to adult CMs[1,30]. Using qualitative and quantitative methods, I identified laminin-511/521 as enhancers for CM maturation.

During heart development, it is well known that CMs undergo structural changes, leading to their adult phenotypes. The growth of the embryonic heart relies on CM proliferation[95]. Postnatally, the endogenous proliferative capacity diminishes, and physiological hypertrophic growth becomes dominant, leading to an increase in

cell size (around 30- to 40-fold in both rodents and human) and binuclear cells[31,44]. In mice, the proportion of binuclear cells increases after birth to adult hearts (1.5% to 91.5%, respectively)[32]. Consistently, PSC-CMs plated on laminin-511/521 were increased cell size, and also showed higher proportions of binuclear cells than gelatin (gelatin, 7.77%; laminin-511, 38.68%; laminin-521, 54.72%). Moreover, PSC-CMs cultured on laminin-511/521 were also increased sarcomere length (gelatin, ~1.91 μm; laminin-511, ~1.99 μm; laminin-521, ~1.97 μm). In agreement with this result, the sarcomere length of CMs is increased from fetal to adult stage (fetal CMs, ~1.6 μm; adult CMs, ~2.2 μm)[30]. In addition, Cx43 localization also considered as a hallmark for CM maturation. In embryonic, Cx43 diffusely expresses in the cytoplasm, whereas it localizes to the lateral cell-axis in neonate stage. Since the CMs reach to mature stage, Cx43 mostly localizes to intercalated disk[11]. In this study, the result showed that PSC-CMs plated on laminin-511/521 promoted localization of Cx43 to lateral cell-axis. Along with transcriptome analysis, the maturation scores of the PSC-CMs plated on laminin-511/521 were comparable to P7 and P14 heart. Altogether, laminin-511/521 enhanced the maturity of PSC-CMs equivalent to postnatal heart.

Laminins consist of three chains termed α, β, and γ. The laminin proteins are named in accordance with their chain compositions. For instance, laminin-511 composes of α5, β1, and γ1 chains[96]. Laminin E8 fragments are minimal forms of intact laminins, which contain C-terminal regions of the α, β, and γ chains. These minimal fragments contain the active integrin-binding site, which consists of laminin globular 1-3 domains of α subunit and the glutamate residue at C-terminal tail of the γ chain[97], but absent other parts such as heparin/heparan sulphate-binding region[98]. Thus, the laminin E8 fragments retain the full capacity of binding to integrins similar to intact laminins[99]. Integrins are transmembrane receptors, contributing to cell-ECM proteins and cell-cell adhesion. Integrin-binding ECMs are able to activate several intracellular signaling cascades, which relate to cell survival, proliferation, motility, and differentiation[100–103]. Previous study has shown that the interactions between laminin-511/521 E8 fragments are primarily α6β1 integrin-dependent, by which blocking of α6β1 integrin suppressed adhesion of cells to those laminins[104]. Moreover, a mutant laminin-511 E8 fragment lost their binding affinity to α6β1 integrin, even though a single amino-acid substitution[97]. Thus, I believe that the interactions of laminin-

511/521 with α6β1 integrin are the important route for cell-ECM binding and enhancing PSC-CMs maturation.

Although PSC-CMs displayed more mature phenotypes on laminin-511/521, these cells were still immature compared to adult CMs. As developing CM are exposed to combinatorial effects of several environmental cues such as hormones, substrate stiffness, and electrical stimulation, combinations of these environmental cues would likely lead the PSC-CMs mature like adult CMs.

Acknowledgments

I gratefully acknowledge technical supports and helpful discussions from all members in Regenerative Medicine including Prof.Yutaka Hanazono, Hideki Uosaki, Tomoyuki Abe, Hiroaki Shibata, Hiromasa Hara, Suvd Byambaa, Rie Ishihara. Mari Karube, and Eri Noguchi.

Funding supports

This work was supported by The Program for Technological Innovation of Regenerative Medicine, Research Center Network for Realization of Regenerative Medicine from Japan Agency for Medical Research and Development (AMED, 18bm0704012h0003), Grant-in-Aid for Early-Career Scientists (19K17613) and Fund for the Promotion of Joint International Research (Fostering Joint International Research (B), 19KK0219) from Japan Society for the Promotion of Science, Novartis Research Grant, Sakakibara Memorial Research Grant from Japan Research Promotion Society for Cardiovascular Diseases, Takeda Science Foundation, The Uehara Memorial Foundation, SENSHIN Medical Research Foundation, and the Grant for Basic Research of the Japanese Circulation Society (to Hideki Uosaki). This work was also partly supported by JMU start-up award and JMU graduate student research award from Jichi Medical University (to me, Nawin Chanthra).

References

1. Uosaki, H., Cahan, P., Lee, D. I., Wang, S., Miyamoto, M., Fernandez, L., Kass, D. A. & Kwon, C. Transcriptional Landscape of Cardiomyocyte Maturation. *Cell Rep.* **13,** 1705–1716 (2015).
2. Till, J. E. & McCULLOCH, E. A. A direct measurement of the radiation sensitivity of normal mouse bone marrow cells. *Radiat. Res.* **14,** 213–222 (1961).
3. Wobus, A. M. & Boheler, K. R. Embryonic stem cells: prospects for developmental biology and cell therapy. *Physiol. Rev.* **85,** 635–678 (2005).
4. Evans, M. J. & Kaufman, M. H. Establishment in culture of pluripotential cells from mouse embryos. *Nature* **292,** 154–156 (1981).
5. Thomson, J. A., Itskovitz-Eldor, J., Shapiro, S. S., Waknitz, M. A., Swiergiel, J. J., Marshall, V. S. & Jones, J. M. Embryonic stem cell lines derived from human blastocysts. *Science* **282,** 1145–1147 (1998).
6. Takahashi, K. & Yamanaka, S. Induction of pluripotent stem cells from mouse embryonic and adult fibroblast cultures by defined factors. *Cell* **126,** 663–676 (2006).
7. Takahashi, K., Tanabe, K., Ohnuki, M., Narita, M., Ichisaka, T., Tomoda, K. & Yamanaka, S. Induction of pluripotent stem cells from adult human fibroblasts by defined factors. *Cell* **131,** 861–872 (2007).
8. Chong, J. J. H. & Murry, C. E. Cardiac regeneration using pluripotent stem cells--progression to large animal models. *Stem Cell Res.* **13,** 654–665 (2014).
9. Uosaki, H., Fukushima, H., Takeuchi, A., Matsuoka, S., Nakatsuji, N., Yamanaka, S. & Yamashita, J. K. Efficient and scalable purification of cardiomyocytes from human embryonic and induced pluripotent stem cells by VCAM1 surface expression. *PloS One* **6,** e23657 (2011).
10. Denning, C., Borgdorff, V., Crutchley, J., Firth, K. S. A., George, V., Kalra, S., Kondrashov, A., Hoang, M. D., Mosqueira, D., Patel, A., Prodanov, L., Rajamohan, D., Skarnes, W. C., Smith, J. G. W. & Young, L. E. Cardiomyocytes from human pluripotent stem cells: From laboratory curiosity to industrial biomedical platform. *Biochim. Biophys. Acta* **1863,** 1728–1748 (2016).
11. Vreeker, A., van Stuijvenberg, L., Hund, T. J., Mohler, P. J., Nikkels, P. G. J. & van Veen, T. A. B. Assembly of the cardiac intercalated disk during pre- and postnatal development of the human heart. *PloS One* **9,** e94722 (2014).

12. Zhang, J., Wilson, G. F., Soerens, A. G., Koonce, C. H., Yu, J., Palecek, S. P., Thomson, J. A. & Kamp, T. J. Functional cardiomyocytes derived from human induced pluripotent stem cells. *Circ. Res.* **104,** e30-41 (2009).
13. Itzhaki, I., Rapoport, S., Huber, I., Mizrahi, I., Zwi-Dantsis, L., Arbel, G., Schiller, J. & Gepstein, L. Calcium handling in human induced pluripotent stem cell derived cardiomyocytes. *PloS One* **6,** e18037 (2011).
14. Germanguz, I., Sedan, O., Zeevi-Levin, N., Shtrichman, R., Barak, E., Ziskind, A., Eliyahu, S., Meiry, G., Amit, M., Itskovitz-Eldor, J. & Binah, O. Molecular characterization and functional properties of cardiomyocytes derived from human inducible pluripotent stem cells. *J. Cell. Mol. Med.* **15,** 38–51 (2011).
15. Gherghiceanu, M., Barad, L., Novak, A., Reiter, I., Itskovitz-Eldor, J., Binah, O. & Popescu, L. M. Cardiomyocytes derived from human embryonic and induced pluripotent stem cells: comparative ultrastructure. *J. Cell. Mol. Med.* **15,** 2539–2551 (2011).
16. Snir, M., Kehat, I., Gepstein, A., Coleman, R., Itskovitz-Eldor, J., Livne, E. & Gepstein, L. Assessment of the ultrastructural and proliferative properties of human embryonic stem cell-derived cardiomyocytes. *Am. J. Physiol. Heart Circ. Physiol.* **285,** H2355-2363 (2003).
17. Karakikes, I., Ameen, M., Termglinchan, V. & Wu, J. C. Human induced pluripotent stem cell-derived cardiomyocytes: insights into molecular, cellular, and functional phenotypes. *Circ. Res.* **117,** 80–88 (2015).
18. Lopaschuk, G. D. & Jaswal, J. S. Energy metabolic phenotype of the cardiomyocyte during development, differentiation, and postnatal maturation. *J. Cardiovasc. Pharmacol.* **56,** 130–140 (2010).
19. Kim, C., Wong, J., Wen, J., Wang, S., Wang, C., Spiering, S., Kan, N. G., Forcales, S., Puri, P. L., Leone, T. C., Marine, J. E., Calkins, H., Kelly, D. P., Judge, D. P. & Chen, H.-S. V. Studying arrhythmogenic right ventricular dysplasia with patient-specific iPSCs. *Nature* **494,** 105–110 (2013).
20. Zhu, W.-Z., Santana, L. F. & Laflamme, M. A. Local control of excitation-contraction coupling in human embryonic stem cell-derived cardiomyocytes. *PloS One* **4,** e5407 (2009).
21. Satin, J., Itzhaki, I., Rapoport, S., Schroder, E. A., Izu, L., Arbel, G., Beyar, R., Balke, C. W., Schiller, J. & Gepstein, L. Calcium handling in human embryonic stem cell-derived cardiomyocytes. *Stem Cells* **26,** 1961–1972 (2008).

22. Liu, J., Fu, J. D., Siu, C. W. & Li, R. A. Functional sarcoplasmic reticulum for calcium handling of human embryonic stem cell-derived cardiomyocytes: insights for driven maturation. *Stem Cells* **25,** 3038–3044 (2007).
23. Liu, J., Lieu, D. K., Siu, C. W., Fu, J.-D., Tse, H.-F. & Li, R. A. Facilitated maturation of Ca2+ handling properties of human embryonic stem cell-derived cardiomyocytes by calsequestrin expression. *Am. J. Physiol. Cell Physiol.* **297,** C152-159 (2009).
24. Janowski, E., Cleemann, L., Sasse, P. & Morad, M. Diversity of Ca2+ signaling in developing cardiac cells. *Ann. N. Y. Acad. Sci.* **1080,** 154–164 (2006).
25. Liu, W., Yasui, K., Opthof, T., Ishiki, R., Lee, J.-K., Kamiya, K., Yokota, M. & Kodama, I. Developmental changes of Ca(2+) handling in mouse ventricular cells from early embryo to adulthood. *Life Sci.* **71,** 1279–1292 (2002).
26. Escobar, A. L., Ribeiro-Costa, R., Villalba-Galea, C., Zoghbi, M. E., Pérez, C. G. & Mejía-Alvarez, R. Developmental changes of intracellular Ca2+ transients in beating rat hearts. *Am. J. Physiol. Heart Circ. Physiol.* **286,** H971-978 (2004).
27. Tanaka, H. & Shigenobu, K. Effect of ryanodine on neonatal and adult rat heart: developmental increase in sarcoplasmic reticulum function. *J. Mol. Cell. Cardiol.* **21,** 1305–1313 (1989).
28. Huang, J., Hove-Madsen, L. & Tibbits, G. F. Ontogeny of Ca2+-induced Ca2+ release in rabbit ventricular myocytes. *Am. J. Physiol. Cell Physiol.* **294,** C516-525 (2008).
29. Veerman, C. C., Kosmidis, G., Mummery, C. L., Casini, S., Verkerk, A. O. & Bellin, M. Immaturity of human stem-cell-derived cardiomyocytes in culture: fatal flaw or soluble problem? *Stem Cells Dev.* **24,** 1035–1052 (2015).
30. Yang, X., Pabon, L. & Murry, C. E. Engineering adolescence: maturation of human pluripotent stem cell-derived cardiomyocytes. *Circ. Res.* **114,** 511–523 (2014).
31. Mollova, M., Bersell, K., Walsh, S., Savla, J., Das, L. T., Park, S.-Y., Silberstein, L. E., Dos Remedios, C. G., Graham, D., Colan, S. & Kühn, B. Cardiomyocyte proliferation contributes to heart growth in young humans. *Proc. Natl. Acad. Sci. U. S. A.* **110,** 1446–1451 (2013).
32. Soonpaa, M. H., Kim, K. K., Pajak, L., Franklin, M. & Field, L. J. Cardiomyocyte DNA synthesis and binucleation during murine development. *Am. J. Physiol.* **271,** H2183-2189 (1996).

33. Lundy, S. D., Zhu, W.-Z., Regnier, M. & Laflamme, M. A. Structural and functional maturation of cardiomyocytes derived from human pluripotent stem cells. *Stem Cells Dev.* **22,** 1991–2002 (2013).
34. Porter, G. A., Hom, J., Hoffman, D., Quintanilla, R., de Mesy Bentley, K. & Sheu, S.-S. Bioenergetics, mitochondria, and cardiac myocyte differentiation. *Prog. Pediatr. Cardiol.* **31,** 75–81 (2011).
35. Feric, N. T. & Radisic, M. Maturing human pluripotent stem cell-derived cardiomyocytes in human engineered cardiac tissues. *Adv. Drug Deliv. Rev.* **96,** 110–134 (2016).
36. Jiang, Y., Park, P., Hong, S.-M. & Ban, K. Maturation of Cardiomyocytes Derived from Human Pluripotent Stem Cells: Current Strategies and Limitations. *Mol. Cells* **41,** 613–621 (2018).
37. Lompre, A. M., Schwartz, K., d'Albis, A., Lacombe, G., Van Thiem, N. & Swynghedauw, B. Myosin isoenzyme redistribution in chronic heart overload. *Nature* **282,** 105–107 (1979).
38. Zhu, H., Scharnhorst, K. S., Stieg, A. Z., Gimzewski, J. K., Minami, I., Nakatsuji, N., Nakano, H. & Nakano, A. Two dimensional electrophysiological characterization of human pluripotent stem cell-derived cardiomyocyte system. *Sci. Rep.* **7,** 43210 (2017).
39. Kadota, S., Minami, I., Morone, N., Heuser, J. E., Agladze, K. & Nakatsuji, N. Development of a reentrant arrhythmia model in human pluripotent stem cell-derived cardiac cell sheets. *Eur. Heart J.* **34,** 1147–1156 (2013).
40. Drouin, E., Charpentier, F., Gauthier, C., Laurent, K. & Le Marec, H. Electrophysiologic characteristics of cells spanning the left ventricular wall of human heart: evidence for presence of M cells. *J. Am. Coll. Cardiol.* **26,** 185–192 (1995).
41. Peters, N. S., Green, C. R., Poole-Wilson, P. A. & Severs, N. J. Reduced content of connexin43 gap junctions in ventricular myocardium from hypertrophied and ischemic human hearts. *Circulation* **88,** 864–875 (1993).
42. Cho, G.-S., Lee, D. I., Tampakakis, E., Murphy, S., Andersen, P., Uosaki, H., Chelko, S., Chakir, K., Hong, I., Seo, K., Chen, H.-S. V., Chen, X., Basso, C., Houser, S. R., Tomaselli, G. F., O'Rourke, B., Judge, D. P., Kass, D. A. & Kwon, C. Neonatal Transplantation Confers Maturation of PSC-Derived Cardiomyocytes Conducive to Modeling Cardiomyopathy. *Cell Rep.* **18,** 571–582 (2017).

43. Peters, N. S., Severs, N. J., Rothery, S. M., Lincoln, C., Yacoub, M. H. & Green, C. R. Spatiotemporal relation between gap junctions and fascia adherens junctions during postnatal development of human ventricular myocardium. *Circulation* **90,** 713–725 (1994).
44. Laflamme, M. A. & Murry, C. E. Heart regeneration. *Nature* **473,** 326–335 (2011).
45. Kamakura, T., Makiyama, T., Sasaki, K., Yoshida, Y., Wuriyanghai, Y., Chen, J., Hattori, T., Ohno, S., Kita, T., Horie, M., Yamanaka, S. & Kimura, T. Ultrastructural maturation of human-induced pluripotent stem cell-derived cardiomyocytes in a long-term culture. *Circ. J.* **77,** 1307–1314 (2013).
46. Sartiani, L., Bettiol, E., Stillitano, F., Mugelli, A., Cerbai, E. & Jaconi, M. E. Developmental changes in cardiomyocytes differentiated from human embryonic stem cells: a molecular and electrophysiological approach. *Stem Cells* **25,** 1136–1144 (2007).
47. Herron, T. J., Rocha, A. M. D., Campbell, K. F., Ponce-Balbuena, D., Willis, B. C., Guerrero-Serna, G., Liu, Q., Klos, M., Musa, H., Zarzoso, M., Bizy, A., Furness, J., Anumonwo, J., Mironov, S. & Jalife, J. Extracellular Matrix-Mediated Maturation of Human Pluripotent Stem Cell-Derived Cardiac Monolayer Structure and Electrophysiological Function. *Circ. Arrhythm. Electrophysiol.* **9,** e003638 (2016).
48. VanWinkle, W. B., Snuggs, M. B. & Buja, L. M. Cardiogel: a biosynthetic extracellular matrix for cardiomyocyte culture. *In Vitro Cell. Dev. Biol. Anim.* **32,** 478–485 (1996).
49. Zhang, J., Klos, M., Wilson, G. F., Herman, A. M., Lian, X., Raval, K. K., Barron, M. R., Hou, L., Soerens, A. G., Yu, J., Palecek, S. P., Lyons, G. E., Thomson, J. A., Herron, T. J., Jalife, J. & Kamp, T. J. Extracellular matrix promotes highly efficient cardiac differentiation of human pluripotent stem cells: the matrix sandwich method. *Circ. Res.* **111,** 1125–1136 (2012).
50. Yang, X., Rodriguez, M., Pabon, L., Fischer, K. A., Reinecke, H., Regnier, M., Sniadecki, N. J., Ruohola-Baker, H. & Murry, C. E. Tri-iodo-l-thyronine promotes the maturation of human cardiomyocytes-derived from induced pluripotent stem cells. *J. Mol. Cell. Cardiol.* **72,** 296–304 (2014).
51. Krüger, M., Sachse, C., Zimmermann, W. H., Eschenhagen, T., Klede, S. & Linke, W. A. Thyroid hormone regulates developmental titin isoform transitions via the phosphatidylinositol-3-kinase/ AKT pathway. *Circ. Res.* **102,** 439–447 (2008).

52. Kosmidis, G., Bellin, M., Ribeiro, M. C., van Meer, B., Ward-van Oostwaard, D., Passier, R., Tertoolen, L. G. J., Mummery, C. L. & Casini, S. Altered calcium handling and increased contraction force in human embryonic stem cell derived cardiomyocytes following short term dexamethasone exposure. *Biochem. Biophys. Res. Commun.* **467,** 998–1005 (2015).
53. Parikh, S. S., Blackwell, D. J., Gomez-Hurtado, N., Frisk, M., Wang, L., Kim, K., Dahl, C. P., Fiane, A., Tønnessen, T., Kryshtal, D. O., Louch, W. E. & Knollmann, B. C. Thyroid and Glucocorticoid Hormones Promote Functional T-Tubule Development in Human-Induced Pluripotent Stem Cell-Derived Cardiomyocytes. *Circ. Res.* **121,** 1323–1330 (2017).
54. Jacot, J. G., Martin, J. C. & Hunt, D. L. Mechanobiology of cardiomyocyte development. *J. Biomech.* **43,** 93–98 (2010).
55. Prakash, Y. S., Cody, M. J., Housmans, P. R., Hannon, J. D. & Sieck, G. C. Comparison of cross-bridge cycling kinetics in neonatal vs. adult rat ventricular muscle. *J. Muscle Res. Cell Motil.* **20,** 717–723 (1999).
56. Bajaj, P., Tang, X., Saif, T. A. & Bashir, R. Stiffness of the substrate influences the phenotype of embryonic chicken cardiac myocytes. *J. Biomed. Mater. Res. A* **95,** 1261–1269 (2010).
57. Jacot, J. G., McCulloch, A. D. & Omens, J. H. Substrate stiffness affects the functional maturation of neonatal rat ventricular myocytes. *Biophys. J.* **95,** 3479–3487 (2008).
58. Berry, M. F., Engler, A. J., Woo, Y. J., Pirolli, T. J., Bish, L. T., Jayasankar, V., Morine, K. J., Gardner, T. J., Discher, D. E. & Sweeney, H. L. Mesenchymal stem cell injection after myocardial infarction improves myocardial compliance. *Am. J. Physiol. Heart Circ. Physiol.* **290,** H2196-2203 (2006).
59. McCain, M. L. & Parker, K. K. Mechanotransduction: the role of mechanical stress, myocyte shape, and cytoskeletal architecture on cardiac function. *Pflugers Arch.* **462,** 89–104 (2011).
60. Rodriguez, A. G., Han, S. J., Regnier, M. & Sniadecki, N. J. Substrate stiffness increases twitch power of neonatal cardiomyocytes in correlation with changes in myofibril structure and intracellular calcium. *Biophys. J.* **101,** 2455–2464 (2011).
61. Engler, A. J., Carag-Krieger, C., Johnson, C. P., Raab, M., Tang, H.-Y., Speicher, D. W., Sanger, J. W., Sanger, J. M. & Discher, D. E. Embryonic cardiomyocytes

beat best on a matrix with heart-like elasticity: scar-like rigidity inhibits beating. *J. Cell Sci.* **121,** 3794–3802 (2008).

62. Asahi, M., Otsu, K., Nakayama, H., Hikoso, S., Takeda, T., Gramolini, A. O., Trivieri, M. G., Oudit, G. Y., Morita, T., Kusakari, Y., Hirano, S., Hongo, K., Hirotani, S., Yamaguchi, O., Peterson, A., Backx, P. H., Kurihara, S., Hori, M. & MacLennan, D. H. Cardiac-specific overexpression of sarcolipin inhibits sarco(endo)plasmic reticulum Ca2+ ATPase (SERCA2a) activity and impairs cardiac function in mice. *Proc. Natl. Acad. Sci. U. S. A.* **101,** 9199–9204 (2004).
63. Radisic, M., Park, H., Shing, H., Consi, T., Schoen, F. J., Langer, R., Freed, L. E. & Vunjak-Novakovic, G. Functional assembly of engineered myocardium by electrical stimulation of cardiac myocytes cultured on scaffolds. *Proc. Natl. Acad. Sci. U. S. A.* **101,** 18129–18134 (2004).
64. Sathaye, A., Bursac, N., Sheehy, S. & Tung, L. Electrical pacing counteracts intrinsic shortening of action potential duration of neonatal rat ventricular cells in culture. *J. Mol. Cell. Cardiol.* **41,** 633–641 (2006).
65. Xia, Y., Buja, L. M., Scarpulla, R. C. & McMillin, J. B. Electrical stimulation of neonatal cardiomyocytes results in the sequential activation of nuclear genes governing mitochondrial proliferation and differentiation. *Proc. Natl. Acad. Sci. U. S. A.* **94,** 11399–11404 (1997).
66. Nunes, S. S., Miklas, J. W., Liu, J., Aschar-Sobbi, R., Xiao, Y., Zhang, B., Jiang, J., Massé, S., Gagliardi, M., Hsieh, A., Thavandiran, N., Laflamme, M. A., Nanthakumar, K., Gross, G. J., Backx, P. H., Keller, G. & Radisic, M. Biowire: a platform for maturation of human pluripotent stem cell-derived cardiomyocytes. *Nat. Methods* **10,** 781–787 (2013).
67. You, J.-O., Rafat, M., Ye, G. J. C. & Auguste, D. T. Nanoengineering the heart: conductive scaffolds enhance connexin 43 expression. *Nano Lett.* **11,** 3643–3648 (2011).
68. Zhou, P. & Pu, W. T. Recounting Cardiac Cellular Composition. *Circ. Res.* **118,** 368–370 (2016).
69. Kim, C., Majdi, M., Xia, P., Wei, K. A., Talantova, M., Spiering, S., Nelson, B., Mercola, M. & Chen, H.-S. V. Non-cardiomyocytes influence the electrophysiological maturation of human embryonic stem cell-derived cardiomyocytes during differentiation. *Stem Cells Dev.* **19,** 783–795 (2010).

70. Gao, L., Gregorich, Z. R., Zhu, W., Mattapally, S., Oduk, Y., Lou, X., Kannappan, R., Borovjagin, A. V., Walcott, G. P., Pollard, A. E., Fast, V. G., Hu, X., Lloyd, S. G., Ge, Y. & Zhang, J. Large Cardiac Muscle Patches Engineered From Human Induced-Pluripotent Stem Cell-Derived Cardiac Cells Improve Recovery From Myocardial Infarction in Swine. *Circulation* **137,** 1712–1730 (2018).
71. Ruan, J.-L., Tulloch, N. L., Razumova, M. V., Saiget, M., Muskheli, V., Pabon, L., Reinecke, H., Regnier, M. & Murry, C. E. Mechanical Stress Conditioning and Electrical Stimulation Promote Contractility and Force Maturation of Induced Pluripotent Stem Cell-Derived Human Cardiac Tissue. *Circulation* **134,** 1557–1567 (2016).
72. Shadrin, I. Y., Allen, B. W., Qian, Y., Jackman, C. P., Carlson, A. L., Juhas, M. E. & Bursac, N. Cardiopatch platform enables maturation and scale-up of human pluripotent stem cell-derived engineered heart tissues. *Nat. Commun.* **8,** 1825 (2017).
73. Chan, H. Y. S., Keung, W., Li, R. A., Miller, A. L. & Webb, S. E. Morphometric Analysis of Human Embryonic Stem Cell-Derived Ventricular Cardiomyocytes: Determining the Maturation State of a Population by Quantifying Parameters in Individual Cells. *Stem Cells Int.* **2015,** 586908 (2015).
74. Hayes, H. B., Nicolini, A. M., Arrowood, C. A., Chvatal, S. A., Wolfson, D. W., Cho, H. C., Sullivan, D. D., Chal, J., Fermini, B., Clements, M., Ross, J. D. & Millard, D. C. Novel method for action potential measurements from intact cardiac monolayers with multiwell microelectrode array technology. *Sci. Rep.* **9,** 11893 (2019).
75. Sasaki, D., Matsuura, K., Seta, H., Haraguchi, Y., Okano, T. & Shimizu, T. Contractile force measurement of human induced pluripotent stem cell-derived cardiac cell sheet-tissue. *PloS One* **13,** e0198026 (2018).
76. Horikoshi, Y., Yan, Y., Terashvili, M., Wells, C., Horikoshi, H., Fujita, S., Bosnjak, Z. J. & Bai, X. Fatty Acid-Treated Induced Pluripotent Stem Cell-Derived Human Cardiomyocytes Exhibit Adult Cardiomyocyte-Like Energy Metabolism Phenotypes. *Cells* **8,** (2019).
77. Den Hartogh, S. C. & Passier, R. Concise Review: Fluorescent Reporters in Human Pluripotent Stem Cells: Contributions to Cardiac Differentiation and Their Applications in Cardiac Disease and Toxicity. *Stem Cells* **34,** 13–26 (2016).

78. Yamanaka, S., Zahanich, I., Wersto, R. P. & Boheler, K. R. Enhanced proliferation of monolayer cultures of embryonic stem (ES) cell-derived cardiomyocytes following acute loss of retinoblastoma. *PloS One* **3,** e3896 (2008).
79. Uosaki, H., Andersen, P., Shenje, L. T., Fernandez, L., Christiansen, S. L. & Kwon, C. Direct contact with endoderm-like cells efficiently induces cardiac progenitors from mouse and human pluripotent stem cells. *PloS One* **7,** e46413 (2012).
80. Kattman, S. J., Witty, A. D., Gagliardi, M., Dubois, N. C., Niapour, M., Hotta, A., Ellis, J. & Keller, G. Stage-specific optimization of activin/nodal and BMP signaling promotes cardiac differentiation of mouse and human pluripotent stem cell lines. *Cell Stem Cell* **8,** 228–240 (2011).
81. Ran, F. A., Hsu, P. D., Wright, J., Agarwala, V., Scott, D. A. & Zhang, F. Genome engineering using the CRISPR-Cas9 system. *Nat. Protoc.* **8,** 2281–2308 (2013).
82. Dobin, A., Davis, C. A., Schlesinger, F., Drenkow, J., Zaleski, C., Jha, S., Batut, P., Chaisson, M. & Gingeras, T. R. STAR: ultrafast universal RNA-seq aligner. *Bioinformatics* **29,** 15–21 (2013).
83. Liao, Y., Smyth, G. K. & Shi, W. featureCounts: an efficient general purpose program for assigning sequence reads to genomic features. *Bioinformatics* **30,** 923–930 (2014).
84. Love, M. I., Huber, W. & Anders, S. Moderated estimation of fold change and dispersion for RNA-seq data with DESeq2. *Genome Biol.* **15,** 550 (2014).
85. Yu, G., Wang, L.-G., Han, Y. & He, Q.-Y. clusterProfiler: an R package for comparing biological themes among gene clusters. *Omics* **16,** 284–287 (2012).
86. Muto, A., Ohkura, M., Abe, G., Nakai, J. & Kawakami, K. Real-time visualization of neuronal activity during perception. *Curr. Biol.* **23,** 307–311 (2013).
87. Pasqualin, C., Gannier, F., Yu, A., Malécot, C. O., Bredeloux, P. & Maupoil, V. SarcOptiM for ImageJ: high-frequency online sarcomere length computing on stimulated cardiomyocytes. *Am. J. Physiol. Cell Physiol.* **311,** C277-283 (2016).
88. Tirosh-Finkel, L., Zeisel, A., Brodt-Ivenshitz, M., Shamai, A., Yao, Z., Seger, R., Domany, E. & Tzahor, E. BMP-mediated inhibition of FGF signaling promotes cardiomyocyte differentiation of anterior heart field progenitors. *Development* **137,** 2989–3000 (2010).
89. Wang, J., Greene, S. B., Bonilla-Claudio, M., Tao, Y., Zhang, J., Bai, Y., Huang, Z., Black, B. L., Wang, F. & Martin, J. F. Bmp signaling regulates myocardial

differentiation from cardiac progenitors through a MicroRNA-mediated mechanism. *Dev. Cell* **19,** 903–912 (2010).

90. Masaki, T. & Takaiti, O. M-protein. *J. Biochem. (Tokyo)* **75,** 367–380 (1974).
91. Noguchi, J., Yanagisawa, M., Imamura, M., Kasuya, Y., Sakurai, T., Tanaka, T. & Masaki, T. Complete primary structure and tissue expression of chicken pectoralis M-protein. *J. Biol. Chem.* **267,** 20302–20310 (1992).
92. Obermann, W. M., Gautel, M., Steiner, F., van der Ven, P. F., Weber, K. & Fürst, D. O. The structure of the sarcomeric M band: localization of defined domains of myomesin, M-protein, and the 250-kD carboxy-terminal region of titin by immunoelectron microscopy. *J. Cell Biol.* **134,** 1441–1453 (1996).
93. Steiner, F., Weber, K. & Fürst, D. O. Structure and expression of the gene encoding murine M-protein, a sarcomere-specific member of the immunoglobulin superfamily. *Genomics* **49,** 83–95 (1998).
94. Zemljic-Harpf, A. E., Godoy, J. C., Platoshyn, O., Asfaw, E. K., Busija, A. R., Domenighetti, A. A. & Ross, R. S. Vinculin directly binds zonula occludens-1 and is essential for stabilizing connexin-43-containing gap junctions in cardiac myocytes. *J. Cell Sci.* **127,** 1104–1116 (2014).
95. Li, F., Wang, X., Capasso, J. M. & Gerdes, A. M. Rapid transition of cardiac myocytes from hyperplasia to hypertrophy during postnatal development. *J. Mol. Cell. Cardiol.* **28,** 1737–1746 (1996).
96. Aumailley, M., Bruckner-Tuderman, L., Carter, W. G., Deutzmann, R., Edgar, D., Ekblom, P., Engel, J., Engvall, E., Hohenester, E., Jones, J. C. R., Kleinman, H. K., Marinkovich, M. P., Martin, G. R., Mayer, U., Meneguzzi, G., Miner, J. H., Miyazaki, K., Patarroyo, M., Paulsson, M., Quaranta, V., Sanes, J. R., Sasaki, T., Sekiguchi, K., Sorokin, L. M., Talts, J. F., Tryggvason, K., Uitto, J., Virtanen, I., von der Mark, K., Wewer, U. M., Yamada, Y. & Yurchenco, P. D. A simplified laminin nomenclature. *Matrix Biol. J. Int. Soc. Matrix Biol.* **24,** 326–332 (2005).
97. Ido, H., Nakamura, A., Kobayashi, R., Ito, S., Li, S., Futaki, S. & Sekiguchi, K. The requirement of the glutamic acid residue at the third position from the carboxyl termini of the laminin gamma chains in integrin binding by laminins. *J. Biol. Chem.* **282,** 11144–11154 (2007).
98. Ido, H., Harada, K., Futaki, S., Hayashi, Y., Nishiuchi, R., Natsuka, Y., Li, S., Wada, Y., Combs, A. C., Ervasti, J. M. & Sekiguchi, K. Molecular dissection of the alpha-

dystroglycan- and integrin-binding sites within the globular domain of human laminin-10. *J. Biol. Chem.* **279,** 10946–10954 (2004).

99. Miyazaki, T., Futaki, S., Suemori, H., Taniguchi, Y., Yamada, M., Kawasaki, M., Hayashi, M., Kumagai, H., Nakatsuji, N., Sekiguchi, K. & Kawase, E. Laminin E8 fragments support efficient adhesion and expansion of dissociated human pluripotent stem cells. *Nat. Commun.* **3,** 1236 (2012).
100. Hynes, R. O. Integrins: bidirectional, allosteric signaling machines. *Cell* **110,** 673–687 (2002).
101. Perrucci, G. L., Rurali, E. & Pompilio, G. Cardiac fibrosis in regenerative medicine: destroy to rebuild. *J. Thorac. Dis.* **10,** S2376–S2389 (2018).
102. Perrucci, G. L., Zanobini, M., Gripari, P., Songia, P., Alshaikh, B., Tremoli, E. & Poggio, P. Pathophysiology of Aortic Stenosis and Mitral Regurgitation. *Compr. Physiol.* **7,** 799–818 (2017).
103. Perrucci, G. L., Barbagallo, V. A., Corlianò, M., Tosi, D., Santoro, R., Nigro, P., Poggio, P., Bulfamante, G., Lombardi, F. & Pompilio, G. Integrin αvβ5 in vitro inhibition limits pro-fibrotic response in cardiac fibroblasts of spontaneously hypertensive rats. *J. Transl. Med.* **16,** 352 (2018).
104. Polisetti, N., Sorokin, L., Okumura, N., Koizumi, N., Kinoshita, S., Kruse, F. E. & Schlötzer-Schrehardt, U. Laminin-511 and -521-based matrices for efficient ex vivo-expansion of human limbal epithelial progenitor cells. *Sci. Rep.* **7,** 5152 (2017).